

Laser Nitrided and TiN Coated Ti-6Al-4V Alloy Surfaces

Omar A. Al-Mana

M.Eng

2011

Laser Nitrided and TiN Coated Ti-6Al-4V Alloy Surfaces

By

Omar Abdul Aziz Al-Mana

BSc in Mechanical Engineering (KFUPM) KSA, 2006

This thesis is submitted to Dublin City University as the fulfillment of the
requirement for award of degree of

Masters of Engineering (M.Eng)

Research Supervisors

Professor M.S.J. Hashmi (Ph.D, D.Sc, CEng., FIMechE., FIEI, MASME)

Professor B.S. Yilbas (Ph.D, D.Eng., MASME)

**School of Mechanical & Manufacturing Engineering
Dublin City University**

January 2011

DECLARATION

I hereby certify that this material, which I now submit for assessment on the programme of study leading to the award of Master's of Engineering (MEng) is entirely my own work, that I have exercised reasonable care to ensure that the work is original, and does not to the best of my knowledge breach any law of copyright, and has not been taken from the work of others save and to the extent that such work has been cited and acknowledged within the text of my work.

Signed: 

ID No. 57127344

Date: 1/18/2011

ACKNOWLEDGEMENTS

I would like to express my gratefulness to my supervisors, **Professor M.S.J. Hashmi** and **Professor B.S. Yilbas** for their close guidance and support during my study.

Also, I am truthfully grateful to my father, mother, brothers and sisters for their prayers and support. And special appreciation to my beloved wife **Mashael** for her encouragements and patience during my long hours of work and studying and keeping me motivated throughout the whole period.

This work would not have been possible without the mentorship of **Dr. Hussain Al-Fadhli**, for committing himself and dedicating much of his personal time and efforts in order to support my study.

I am sincerely thankful for my colleagues who assisted me in this work including **Dr. Ihsan Taie**, and **Meshari Ghannam**.

Lastly, I would like to extend my thanks to all of my friends for their encouragement and support

Title of Thesis: Laser Nitrided and TiN Coated Ti-6Al-4V Alloy surfaces

Name of Student: Omar A. Al-Mana **Student Number:** 57127344

ABSTRACT

Titanium alloys are widely used in aerospace industry due to their low density and high toughness to mass ratios. However, the wear resistance of the titanium alloys is poor and requires surface treatment for the effective usage. One of the methods to improve the surface properties is to nitride the surface forming the nitride rich compounds in the surface region. Titanium nitrides provide the hard surfaces and improve the tribological properties of the surface. The gas assisted laser nitriding of the titanium alloy surface is desirable, since it involves with fast processing, precision of operation, and low cost. TiN PVD coating of the surface of the nitrided layer reduces the surface roughness and further improves the surface properties through forming a hard envelope at the surface. Consequently, laser gas assisted nitriding of Ti-6Al-4V alloy is carried out. The nitrided surfaces are TiN PVD coated in the coating unit. The melt depth layer is predicted using the analytical formulation. The maximum coating thickness achieved is in the order of 2 μm and maximum nitrided depth layer is 80 μm . It is found that the laser gas assisted nitriding provides a uniform thickness of the treated layer below the surface. The nitrided layer is free from the cracks and other defects such as porous and cavities. The TiN coating at the surface modifies the surface roughness and the elastic modulus of the nitrided layer. In this case, surface roughness reduces slightly and elastic modulus of the treated layer increases. The predictions of the melt layer depth agree with the experimental data.

Table of Contents

	<i>Page</i>
Declaration	I
Acknowledgements	II
Abstract	III
Table of Contents	IV
List of Tables	VI
List of Figure	VII
Nomenclature.....	VIII
Chapter 1 – Introduction.....	1
1.1 Historical Background.....	1
1.2 Properties and Uses of Titanium Alloys.....	1
1.3 Surface Engineering of Titanium Alloys.....	5
1.4 Project Objectives and Thesis Outline.....	8
Chapter 2 – Literature Survey.....	10
2.1 Introduction.....	10
2.2 The Affect of the Laser Nitriding Process Parameters	10
2.3 The Improvement of Wear resistance and Hardness	15
2.4 Resistance Improvement.....	23
2.5 Titanium Nitriding in the Atmosphere	25
2.5 Literature Survey Summary	27
Chapter 3 – Equipment and Procedure.....	29
3.1 Introduction.....	29

3.2 PVD TiN Coating	29
3.3 Workpiece Material (Ti-6Al-4V alloy).....	30
3.4 Material Characterization.....	31
3.4.1 SEM and EDS.....	32
3.4.2 X-ray Diffraction Analysis.....	33
3.5 CO ₂ Laser Melting.....	34
3.6 Hardness Tests.....	36
3.7 Three Point Bending Tests.....	36
3.7.1 Determining Young's Modulus by Three Point Bending.....	37
Chapter 4 – Mathematical Analysis for Laser Melting.....	40
4.1 Introduction.....	40
4.2 Melt Depth Formulation.....	41
Chapter 5 – Results and Discussion.....	44
Chapter 6 – Conclusions and future Work.....	61
Suggestions for Future Work.....	64
Appendix.....	65
References.....	77
Publications by the author.....	80

List of Tables

		<i>Page</i>
1.1	Physical Properties of titanium	1
1.2	Common alloying elements and their stabilizing effect.....	5
3.1	Chemical composition of Ti-6Al-4V Alloy (wt. %).	30
3.2	Laser assisted nitriding conditions.....	35
3.3	Data used in the calculations of Young's modulus from three-point bending tests.....	39
4.1	Workpiece and assisting gas properties used in the simulations	43
5.1	Elastic modulus determined from three-point bending tests	58

List of Figures

	<i>Page</i>
1.1 The difference between bcc (a) and hcp (b) crystal structures.....	4
3.1 JSM-6460LV scanning electron microscope	32
3.2 Bruker XRD D8 Advanced	33
3.3 Experimental Set-up.....	35
3.4 A schematic view of the three point bending test.....	39
5.1 Melt depth thickness with laser power intensity.....	45
5.2 SEM and optical micrographs of top surface of laser nitrided and laser nitrided and TiN coated workpieces.....	47
5.3 SEM micrographs of cross-section of laser nitrided and laser nitrided and TiN coated workpieces.....	50
5.4 diffractogram for laser nitrided Workpiece.....	52
5.5 Microhardness distribution inside laser nitrided workpiece...	53
5.6 Top view of laser nitrided surface.....	55
5.7 Surface roughness of laser nitrided and TiN coated, and laser nitrided workpiece surfaces.....	56
5.8 Load displacement characteristics of three-point bending tests.....	58
5.9 SEM and optical micrographs of surfaces after three-point bending tests.....	60
A.1 A schematic view of liquid and gas side velocities in the coordinate system.....	76

Nomenclature

A	Cross Section area(m^2)
b	Sample width (m)
C_{H_c}	Heat transfer coefficient due to chemical reaction
C_{H_d}	Heat transfer coefficient due to diffusion
C_f	Skin friction coefficient
C_p	Specific heat capacity (J/kgK)
C_{p_g}	Specific heat capacity of assisting gas (J/kgK)
C_{p_m}	Specific heat capacity of liquid (J/kgK)
C_{p_s}	Specific heat capacity of solid (J/kgK)
D	Diffusion coefficient (m^2/s)
d	Displacement of substrate material and coating during the bending test
$\dot{E}_{conduction}$	Rate of energy conducted (W)
$\dot{E}_{convection}$	Rate of energy convected (W)
\dot{E}_{in}	Laser power available at liquid surface (W)
E_c	Elastic modulus of coating (GPa)
E_s	Elastic modulus of substrate (GPa)
\dot{E}_{req}	Rate of energy required to generate melt flow rate (W)
\dot{E}_{melt}	Rate of energy required for melting (W)
h	Heat transfer coefficient (W/m^2K)
h_c	Coating thickness (m)
h_s	Substrate thickness (m)
h_g	Total enthalpy at assisting gas-liquid interface (J/kgK)
h_o	Total enthalpy at boundary edge layer (J/kgK)
I_c	Coating moment of inertia (m^4)
I_s	Substrate moment of inertia (m^4)
k_m	Thermal conductivity of melt layer (W/mK)
l	Distance between the bending test supports (m)
L_{ev}	Substrate latent heat of evaporation (J/kg)
L_m	Substrate latent heat of melting (J/kg)
\dot{m}_g	Assisting gas mass flow rate (kg/s)
\dot{m}_L	Liquid mass flow rate (kg/s)
P	Applied load (N)
Pr	Prandlt number
P_o	Laser output power reaching melt surface after reflection (W)

q_c	Heat transfer rate per unit area of molten metal (J/sm ²)
Ra	Surface roughness
Re	Reynolds number of assisting gas flowing over molten metal
S	Distance along the workpiece surface (m)
Sc	Schmidt number
T_i	Initial temperature of solid substrate (K)
T_m	Melting temperature of solid substrate (K)
T_{oe}	Gas temperature at the edge of boundary layer (K)
T_{oi}	Initial temperature of the workpiece (K)
U_e	Gas velocity at the edge of the gas boundary layer (m/s)
U_L	Melt velocity (m/s)
U_{LS}	Melt velocity at the melt surface (m/s)
V_L	Melt velocity normal to the surface (m/s)

Greek

β	Evaporation factor <1
ρ_e	Assisting Gas density (kg/m ³)
ρ_L	Melt density (kg/m ³)
τ_L	Shear stress exerted by liquid layer on gas layer (Pa)
τ_g	Shear stress exerted by assisting gas on liquid layer (Pa)
δ_L	Liquid layer thickness (m)
σ_b	Bending strength

CHAPTER – 1

Introduction

1.1 Historical Background

Titanium was introduced as an element 200 years ago. In the late 1940's the mechanical and physical properties, along with the alloying characteristics of titanium were identified. Since then, its commercial importance started [1]. The metal titanium is considered to be the ninth most abundant element on earth's surface, and it comes in fourth after aluminum, iron and magnesium in terms of structural metal profusion. It is a silvery-grey metal with high melting point and a relatively low density, about 60% less than steels [2]; Table- 1.1 gives some of the physical properties of titanium.

Name Of element	Atomic Symbol	Atomic Number	Atomic Weight	Density (g/cm ³)	Boiling point (°C)	Melting Point (°C)
Titanium	Ti	22	47.90	4.5	3130	1812

Table- 1.1 Physical Properties of titanium [3]

1.2 Properties and Uses of Titanium Alloys

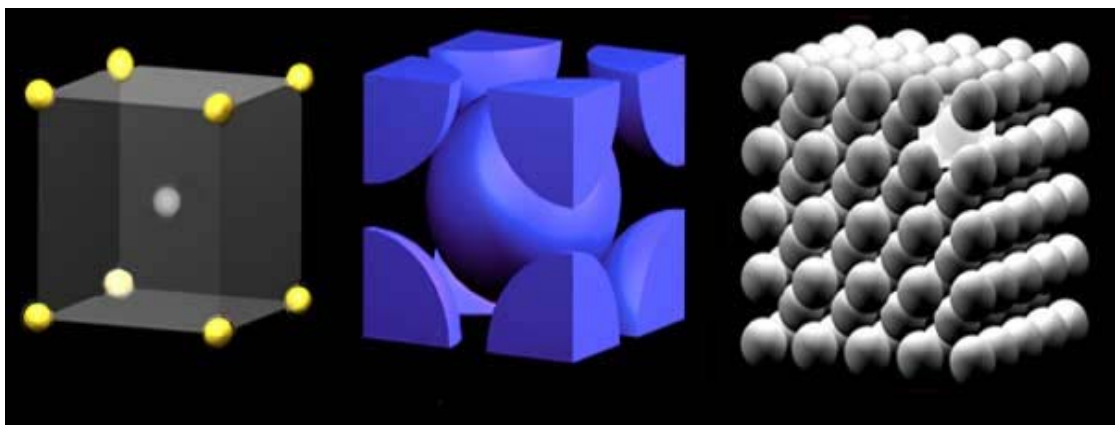
Besides the high toughness to mass ratio of titanium alloys, they have excellent resistance to corrosion. This is due to the presence of a protective strongly adherent titanium oxide film on the surface. This film is usually transparent and titanium has the ability of healing and reproducing this film

instantly in any environment with a presence of oxygen and moisture. Titanium alloys are considered to be very stable and can be attacked by few substances mostly hydrofluoric acid. They are unique in their ability to handle specific chemicals such as chlorine, chlorine chemicals, and chlorides [2]. Also, titanium alloys are biocompatible and they are non toxic and resistant to body fluids corrosion. Such properties made titanium alloys suitable to be used in body implants, such as hip and knee prostheses, bone plates, screws and nails for fractures, pacemaker housing and heart valves[1].

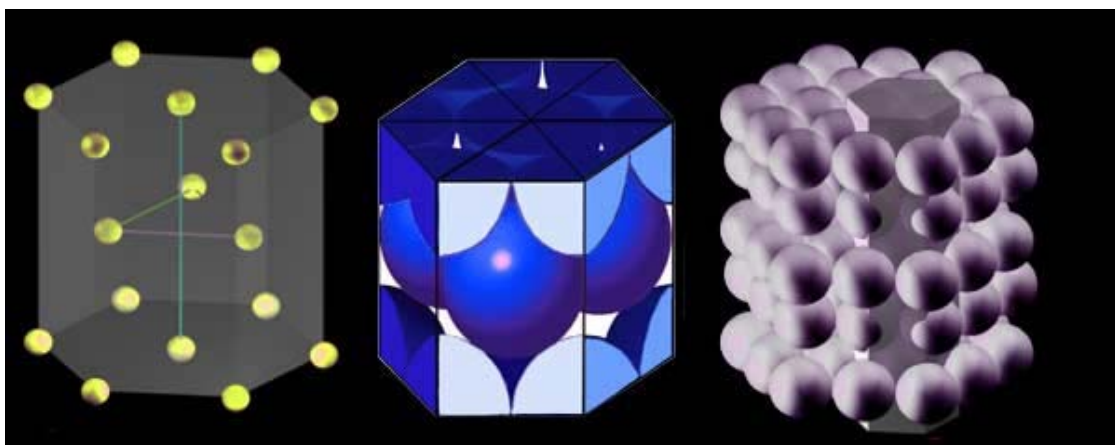
The combination of high strength to weight ratio and the ability to operate at elevated temperatures made titanium alloys attractive to be used in aerospace and aircraft industry. They are widely used in the components of the jet engines, such as the compressor rings, ducts and shrouds, and in the airplane structural components, such fuselage frames, engine mounts, control mechanism parts, sheets and fasteners for the outer body construction [1]. Commercially pure titanium is more commonly used than its alloys for corrosion resistance especially when there is no requirement for high strength [2]. Titanium alloys are suitable for chemical processing industries, oil and refining plants. They are mostly used for storage tanks, columns, and heat exchangers where high corrosion resistance to chemicals is required [1]. Some other applications of titanium alloys found in automotive industry, structural and consumer goods [1].

As the titanium industry was growing quickly, the alloying development progressed rapidly. Titanium exists in two crystallographic forms. The commercially pure (un alloyed) titanium at room temperature has a hexagonal close-packed (hcp) crystal structure and referred to as α (alpha) phase [1]. Once the temperature reaches up to 833°C, the crystal structure transforms into body-centered cubic (bcc) structure, which is known as β (beta) phase [1], Figure- 1.1 shows the difference between (hcp) and (bcc) structures. The basis for the development of the wide range of alloys and properties is by manipulating these crystallographic variations through alloying additions and thermo mechanical processing [1]. In general, titanium alloys can be classified as α alloys, β alloys, or $\alpha+\beta$ alloys. Alpha alloys contain α stabilizing elements, such as aluminum and tin, which inhibit the change in the phase transformation temperature or increasing it. These alloys have better creep resistance than β alloys, and preferred to be used in high temperature applications. They are characterized by adequate strength, toughness and weldability, but poorer forgeability than β alloys. Also, α alloys cannot be heat-treated to increase its strength; they are usually used in their annealed or recrystallized condition in order to eliminate the residual stress caused by working. An example of α alloys is Ti-5Al-2.5Sn [1]. Beta alloys contain transition elements such as vanadium, niobium and molybdenum. These elements lead to decreasing the temperature of α to β phase transition, and hence assist the development of the β bcc phase. These

alloys have excellent forgeability, hadrenability, and responds easily to heat treatment. Ti-10V-2Fe-3Al is an example of β alloys [1]. Table-1.2 lists the common alloying elements and their stabilizing effect. Alpha + Beta alloys contain compositions which support a mixture of α and β phases. These alloys may contain from 10 to 50 % of β phase at room temperature. Ti-6Al-4V is considered to be the most common $\alpha+\beta$ alloy. Heat treatment can be used to control the properties of these alloys; it is used to adjust the amounts and types of β phase present. Alpha + Beta alloys generally have good formability; except for Ti-6Al-4V in particular has poor formability [1].



(a)



(b)

Figure- 1.1 The difference between bcc (a) and hcp (b) crystal structures [4].

Alloying element	Symbol	Range (wt %)	Effect on structure
Aluminum	Al	2-7	α -stabilizer
Tin	Sn	2-6	α -stabilizer
Vanadium	V	2-20	β -stabilizer
Molybdenum	Mo	2-20	β -stabilizer
Chromium	Cr	2-12	β -stabilizer
Copper	C	2-6	β -stabilizer
Zirconium	Zr	2-8	α and β strengthening

Table- 1.2 Common alloying elements and their stabilizing effect [3]

1.3 Surface Engineering of Titanium Alloys

Besides the great physical properties such as high strength to weight ratio and excellent resistance to corrosion and temperature, titanium and its alloys have poor tribological properties such as poor abrasive wear resistance, poor fretting behavior and high coefficient of friction [3]. Surface engineering of titanium and its alloys through heat treatment, coating and thermochemical treatments were found to enhance their poor tribological properties. As a fundamental metallurgical process of materials, heat treatment of titanium and its alloys can be achieved through plasma and laser surface treatments, and ion implantation [3]. The high heating and cooling rates of these treatments aim to change the microstructure of the surface layer without changing its chemistry. However, in most cases, the thermal hardening of the surface is not effective due to the nature of titanium alloys not being submissive to case hardening methods without changing the its surface composition. Various types of coatings can be used on titanium such as chemical conversion coatings, plating, sprayed

coatings and physical vapor deposition (PVD). The term PVD is a combination of processes including evaporation, ion plating and several forms of sputtering to deposit alloys, metals or compounds on a large variety of substrates. The coating of tool material substrate by reactive sputtering or ion plating of TiN is considered to be the most successful engineering application. Thermochemical treatments are considered to be quite effective because they tend to change the chemistry of the surface layer. Oxidation, carburizing and nitriding are the most popular thermochemical treatments used [3]. An oxide film is the result of oxygen in solution of α -Ti alloy. Moreover, during oxidation, this film becomes tougher and thicker, which gives an extra protection against corrosion [3]. Unfortunately, this process cannot improve the wear resistance significantly because the formed oxide layer is usually brittle and can be easily damaged. Carburizing of titanium and its alloys can be performed in a non-oxidizing environment; the carburized TiC layer creates a wear resistance surface for titanium and its alloys [3]. Nitriding of titanium alloys has been used effectively for protection against wear, since nitrogen is highly soluble in α -Ti alloys, it significantly strengthens the surface layer. Nitriding forms a compound layer of TiN on the top with a hardness reaching up to 3000 HV and Ti₂N beneath with a hardness reaching 1500 HV [3].

Plasma nitriding, ion nitriding, gas nitriding, and laser nitriding are the major types of nitriding being used. Conventional plasma nitriding treatment

occupies the low-energy end-spectrum, and has an advantage of controlling the phase formation and the nitrided layer depth. It usually avoids oxidation and requires short nitriding time periods. PVD and ion nitriding are considered to be the two major plasma processes developed for titanium nitriding synthesis [3]. The main disadvantage of plasma nitriding is reducing the fatigue strength, but reducing the processing temperature can solve problem. The high-energy end-spectrum is occupied by the ion beam nitriding process. Nitrogen and Argon ion beams are used on the exposed treated surface, where the nitrogen attacks the surface of the specimen leading to desorption and sputtering of impurities atoms [3]. Gas nitriding can easily form a harder layer on the surface of the materials; that's why is it considered to be a promising method for engineering applications. It is independent of the sample geometry and does not require special equipments, but it requires long time for nitriding and high temperatures. Laser nitriding forms hard titanium nitride layer by melting the surface using a focused laser beam and feeding the nitrogen through a nozzle into the melt pool. The potential of generating excellent metallurgical bond between the substrate and the hardened surface makes laser nitriding an attractive process.

The Laser gas assisted nitriding provides low processing cost and short operation time with high end product quality. The nitrided layer thickness depends on the laser power setting, laser scanning speed, irradiated beam diameter at the surface, and the nitrogen gas pressure. Although increasing laser

power intensity while reducing laser scanning speed enhances the melt depth thickness, evaporation of the surface becomes unavoidable. Consequently, a care must be taken when selecting the nitriding parameters. However, additional coating the laser nitrided surface with hard film, such as PVD TiN, on the surface provides gradual changes of mechanical properties such as hardness and elastic modulus in addition to protecting the surface from severe corrosion attack.

1.4 Project Objective and Thesis Outline

The laser gas assisted nitrided surface has high surface roughness and it is vulnerable to the crevice corrosion when exposed to electrolytic solutions. PVD TiN coating may reduce the surface roughness of initially laser nitride surfaces while improving surface properties, such as corrosion resistance. Consequently, the objective of the present study is to investigate metallurgical and morphological changes in the region subjected to laser gas assisted nitriding and TiN coating at the nitriding surface. For this purpose, laser gas assisted nitriding of Ti-6Al-4V was carried out. The resulting nitrided surfaces were coated with TiN using the PVD coating facility. The microstructural changes and morphology in the laser-irradiated area were examined using SEM, EDS and XRD. The mathematical model was introduced to formulate the melt layer thickness in the surface region of the workpiece. Moreover, three-point bending tests were carried out to determine the elastic modulus of the laser nitrided and

TiN coated regions at the workpiece surface

The thesis consists of six chapters. The first chapter presents general introduction of titanium alloys and their surface engineering methods. The second chapter reports the literature review of previous work related to laser gas assisted nitriding of Ti-6Al-4V alloy. In chapter three, the experimental part is presented and list of the equipment used in preparing the workpieces and performing the associated experiments are included. The mathematical model to formulate the melt layer thickness in the surface region of the irradiated workpiece is introduced in chapter four and the appendix. The results and discussions are discussed in details in chapter five. Finally, conclusion and future works are presented in the last chapter.

CHAPTER – 2

Literature Survey

2.1 Introduction

In this chapter, the studies which were carried out by various researchers in the laser gas assisted nitriding of Ti-6Al-4V alloy and the findings were taken into consideration. The associated studies of the nitriding process parameters and their impact on the laser nitride characteristics are presented. Furthermore, the wear and chemical resistance improvement of the laser gas assisted nitride Ti-6Al-4V is included. Other studies relevant to the nitriding process in the atmosphere environment are also presented. The published literature and advancements in the laser assisted nitriding of the Ti-6Al-4V alloy are categorized under the relevant sub headings.

2.2 The Effect of the Laser Nitriding Process Parameters

The effect of the laser nitriding parameters on the microstructures, microcracks and microhardness of laser nitrided Ti-6Al-4V was investigated by Abboud et al [5]. The laser nitriding of the samples was

performed using CO₂ laser with a shielding device to supply nitrogen gas and prevent oxidation. When changing the laser scanning speed, it was found that the size of the nitride layer decreased by increasing the scanning speed. Moreover, slower laser speeds resulted in a slight increase in the microhardness of the surface. By diluting the nitrogen in the nitriding process with argon, it was found that the samples produced contained no TiN dendrites and had lower microhardness when they are compared with the samples nitrided in pure nitrogen. The difference in nitrogen gas flow rate during the nitriding process resulted in reducing the availability of nitrogen for dissolution in the melt at lower nitrogen gas flow rates. In conclusion, it was found that at slow scanning speeds and relatively high nitrogen flow rates lead to high surface hardness up to 0.8 mm of depth, moreover, cracks intensity can be significantly decreased by mixing argon with nitrogen, but the surface microhardness will be decreased. In general, increasing the scanning speeds will lead to decreasing the crack intensity and the thickness of the nitride layer formed.

The mixing technology of laser and heated Nitrogen on the Titanium alloy was realized by wafting the activated Nitrogen into the laser molten pool. The surface hardness and the composition of nitrides were examined by Yang et. al[6] along with the analysis of laser

nitridation and surface property improvement. The nitriding radiation source was CD-CO₂ laser while pure nitrogen was utilized as the alloying element to the TC4 titanium alloy sample. Nitrogen was pre-heated and wafted into special equipment before reaching the sample where it was activated by the laser and both hit the sample surface at the same time. The laser was used to activate the nitrogen and melt the surface. XRD was used to test the composition of nitrides while the hardness was measured using the 71 type hardness measurement. The XRD results showed that TiN and TiN₂ were formed on the nitrided sample where TiN was the main component. Different nitrides were formed by using different scanning speeds. It was found that the action time between the laser, nitrogen and substrate has an inverse relation with the scanning speed. Also, increasing the scanning speed will gradually increase the surface hardness up to a specific speed then the relation becomes an inverse relation. The main reason for the hardness improvement was the formation of TiN and the grain refinement around the laser pool during the rapid melting and re-crystallizing process. By using the mixing technology of laser and heated nitrogen gas, TiN were formed in the nitridation area, this laser nitridation can be considered as an interaction between the laser and the activated nitrogen with the

substrate at the same time. Also, the improvement of the surface hardness was due to the formation of TiN and the refined grain size.

The effect of laser surface nitriding on the microstructure, mechanical properties, corrosion resistance of a Ti-6Al-4V alloy was investigated by Biswas et al [7]. The laser nitriding was carried out using a CW laser with the presence of nitrogen gas at a constant scanning speed. SEM micrographs of the top surface showed that the nitriding cause the formation of a defect-free and continuous alloy zone consisting of TiN and α -Ti. It was also observed that by increasing the applied power, the dendrites were marginally coarsened. The atomic force microscopy was used to measure the surface roughness of the nitrided layer, it showed a significant improvement of the surface roughness after nitriding when compared to as received samples. The residual stress evaluated by XRD showed that the compressive stress increases with increasing the applied power and decreasing the gas flow rate. However, when reversing values of the parameters, a tensile stress was developed on the nitrided surface layer. In conclusion, it was noted that laser surface nitriding formed a defect-free nitride zone consisting of TiN and α -Ti, which improved the microhardness of the surface.

Examination of microstructure and properties of TiN coating by reactive spraying through using SEM and XRD was carried out by

Tehara et al [8]. Supersonic DC arc plasma jet generator was used for the reactive spraying of TiN. Pure nitrogen was used at low substrate temperature with low power setting, which resulted in deposition of a dense layer of TiN coating. However, increasing the nitrogen flow rate, discharge current and input power, the coating hardness increased. The high potentials for reactive spraying were achieved by supersonic plasma jet coating in thermodynamic and chemical equilibrium states.

The investigation of different properties of the nitrided layers achieved by Nd:YAG laser in different modes and the analysis of the processed layers was carried out by Santos et. al [9]. The Nd: YAG laser operating in CW and pulsed mode was used to nitride the pure titanium samples. The CW laser mode resulted in rough surface layers. SEM results showed that by changing the scanning speed from 16 to 2 mm/s the layer thickness increases from 20 to 60 μm . Moreover, increasing the scanning speed resulted in shorter interaction time and faster cooling rates. Hence, less nitrogen pick up occurred, which resulted in decreased hardness. In Q-sw mode, porous thin layers (1-2 μm) with low roughness were observed. The lattice parameters of the Q-sw mode were close to the CW, resulting in comparable hardness. When using the pulsed laser mode, it was found that when changing the peak power in the single pulse shape mode from 1 kw to 2 kw, the TiN layers change form rough

and porous to smooth with high crack density. It should be noted that the high cooling rates in laser processing results in the formation of the microcracks. When double pulse shape was used, the cooling rate was decreased which resulted in a crack free layer. The XPS results showed high concentration of nitrogen at the top surface of the nitrided layer, which increased the hardness. In conclusion, titanium nitride layers by Nd:YAG laser were successfully made on pure titanium. The nitriding process in CW mode resulted in rough layer surface and can be considered as a roughening process. Q-sw laser nitriding resulted in thin smooth and porous layers. Moreover, in pulsed laser mode, cracks can be avoided in the nitrided layer by changing the mode from single pulse to double pulse shape.

2.3 The Improvement of Wear resistance and Hardness

The wear tests and the metallurgical changes of a laser-treated TiN coated workpieces were carried out and examined by Yilbas et al [10]. Nitrogen was introduced coaxially with the laser beam at constant speed to treat the Ti-6Al-4V surface. Then, the workpiece was slightly grinded prior to the TiN PVD coating. XRD was used to monitor the nitride compounds while SEM used to examine the workpiece cross-section.

Also, a ball-on-disc test method was used for the wear tests. The friction curve results showed three distinct regions. The friction coefficient increases rapidly in the first region, steady state occurs in the second region and then it increases in the third region. The steady state in the laser treated and TiN coated workpiece is longer, when comparing it with a friction curve of TiN coated workpiece. This is an evident of the occurrence of a smooth transition in plastic shearing resistance between the TiN coating and the base substrate. The microstructure of the laser treated and TiN coated workpiece shows that the dendrite structure is dominant in the laser treated region and then they become smaller in the surface region. The microhardness curve shows that the initial laser treatment generates a hard zone in the surface region of the substrate. The wear tests were carried out and showed that laser treated and TiN coated workpiece give better wear tests results when compared to TiN coated workpiece.

Laser gas nitriding of pure titanium and Ti-6Al-4V alloy in an open system was experimented by Tian et al [11]. The pure titanium and Ti-6Al-4V samples were abraded before being nitrided by using continuous wave CO₂ laser and feeding nitrogen through a coaxially placed nozzle. XRD results showed that the compounds in the nitrided layers are mainly TiN_x, while the micrographs showed a crack and pores

free uniformly distributed coarse and short stick-like titanium nitrides morphology. This was attributed to the experiment condition of processing in an open system. Moreover, the dendritic morphology of the compounds in the transitional layer was an evident that solidification rate has an effect on the microstructure. The microhardness profiles showed that hardness decreases when getting deeper below the surface layer. In conclusion, an XRD result of laser nitriding in an open system confirms that the compounds formed in situ in the coatings are mainly TiN_x . Moreover, the resulting high microhardness and good wear resistance improved the load bearing capability of the base materials.

The structural, tribological and electrochemical properties of TiN layers produced by plasma nitriding and deposited by PVD-CFUBMS were applied on Ti-6Al-4V alloy. The characterization of these properties using XRD, SEM, AFM, micro hardness tests, pin-on-disc tribotester, and potentiodynamic tester were performed by Yetim et al[12]. Ti-6Al-4V (grade 5) specimens were used. The plasma nitriding was performed using DC laser in an evacuated chamber. The Ti interlayer was deposited before the TiN deposition to improve the adhesion between the substrate and the film. The surface topography through AFM images shows larger grain sizes on the plasma nitrided sample when compared to the TiN deposited sample. Also, the TiN deposited sample shows uniform,

smooth, dense and columnar structure, while compound and diffusion layers were observed on the plasma nitrided sample from the SEM micrographs. The XRD shows that the TiN deposited layer has a TiN single stage pattern, while the plasma nitrided sample displays TiN and minor Ti_2N phases. The hardness results showed that both methods improved the surface hardness of the alloy, with the plasma nitrided sample having higher values than the TiN deposited sample. The results of the wear test show that friction coefficient increases as the load increase in the untreated sample. Also, in both surface treatment methods, it was determined that as the load increases the friction coefficient increases due to the pin causing wear of the substrate by breaking the modified layers. The explanation of the lower coefficient values is that hard treated surface contains hard nitrides leading to lower contact area which causes the improvement of the wear resistance. It was observed that both surface treatments improved the wear rate. From the typical polarization curves, it was observed that plasma nitrided and TiN deposited samples have a rise in corrosion potential compared to the untreated sample. Both treated samples and untreated sample were subjected to local pitting corrosion and smaller pits were observed on the treated samples compared to the untreated one. Plasma nitriding and TiN deposition and their effects on wear and corrosion resistance of Ti-6Al-

4V were investigated. It has been observed that both methods increased the surface hardness, and when the friction coefficient of the alloy decreases, the wear resistance increases but with the TiN deposition sample having more friction coefficient and wear rate than the plasma nitrided one. Finally, in the corrosion test almost no significant improvements in the electrochemical properties were shown on the treated surfaces when compared to the untreated surfaces.

Yilbas et. al [13] applied three-point bending test on laser gas assisted nitrided, laser gas assisted nitrided and coated, and heat treated and coated Ti-6Al-4V samples to obtain the Young's modulus of the treated zone from the experimental data. The base material used was Ti-6Al-4V alloy. CO₂ laser in pulse mode was used to irradiate the surface of the workpiece. TiN PVD coating was achieved using triode ion plating equipment. Some specimens were heat treated in a furnace in an argon atmosphere by reaching a temperature of 735°C and holding this temperature for 2 hours. SEM and EDS were used to for material characterization of the nitride surface. The SEM results showed that a uniform and crack free nitride layer of 80 µm thick was achieved. Moreover, a 2 µm uniform layer of TiN coating was realized. After the bending tests, the SEM micrographs revealed closely spaced multicracks formed on the as received and coated, as well as the heat treated and

coated specimens. The cracks were developed within the surface region, and no cracks propagation was observed through the coating interface and into the base material. The deformation of the coating was found to relieve the stress levels at the interface. Also, it had a positive effect on the shear stress relaxation in the same region. The large differences in the elastic modulus of the coating and base material was the result of a shear failure in the surface region of the coated section. It was found that the Young's modulus for the TiN coating region was similar to that of the laser nitride region. However, the heat treatment slightly modified the Young's modulus. In conclusion, three point bend tests of as received and TiN coated, heat treated and coated, laser nitride, and laser nitride and coated samples of Ti-6Al-4V was carried out to determine the Young's modulus. It was found that the laser nitride layer improved the material response to the bending, although it was 80 μm thick.

The effect of using duplex surface treatment coating, diamond coating, and laser-surface alloyed coating on Titanium substrate to study their erosion resistance was evaluated by Fu et al [14]. A microwave plasma-assisted diamond CVD system was used to deposit diamond coating on pure Titanium. Nd-YAG laser was used for laser alloying in a Nitrogen atmosphere. Impacting the specimens with erodents at various velocities in a standard sandblasting apparatus was used for solid particle

erosion testing. Natural angular aluminum sands were accelerated by compressed air to attack the specimens. The erosion test displays a linear relation between mass loss and erosion duration in the untreated Titanium. The erosion resistance of Titanium substrate under low impact velocity can be improved by using duplex treated coating, while the erosion resistance is not significant under high impact velocity. The resistance under high and low velocity of diamond coating is almost the same with the untreated Titanium. The laser treated Titanium shows much higher resistance under high and low impact velocity when compared to untreated Titanium. By using the three types of surface treatments of Titanium to improve the erosion resistance, it was observed that the duplex-treated coating can improve the resistance under low impact velocity, while diamond coating shows low resistance to both high and low impact velocity, and the erosion resistance of high and low impact velocity of laser-treated Titanium significantly improved when compared to untreated Titanium.

The process for surface nitriding by a laser beam and resulting properties were investigated by Ettaqi et al [15]. The surface of the workpieces was hardened using the nitrogen gas flow through laser melting of the pre-deposited TiN powder layer. This provided reactions between titanium, nitrogen gas, and TiN powder layer. The resulting

nitrided surfaces were examined by using the optical microscopy and crystallographic analysis was carried out using X-ray diffraction (XRD). In addition, microhardness measurements were carried out to determine the hardness distribution in the nitrided layer. The tribological tests were also carried out to measure the friction coefficient of the surface. They found that the surface appearance and the surface texture were dependent on the nitriding process and the hardness of the surface remarkably increases after the laser treatment process. Moreover, the wear resistance of the nitrided surface was improved and friction coefficient was determined.

The effect of the laser nitriding parameters on the microstructure, phases, microhardness and the biocompatibility of the nitrided surface of Ti-6Al-4V was investigated by Biswas et. al [16]. The sand blasted Ti-6Al-4V samples were nitrided using CW diode laser with nitrogen as a shrouding gas. SEM and XRD were used to analyze the microstructure and the phases of the nitrided layer, while the microhardness was measured using the Vickers microhardness tester. The SEM micrographs of the nitrided layers showed a formation of highly refined TiN dendrites in the α -Ti matrix. When comparing the XRD analysis of both the as received and the laser nitrided Ti-6Al-4V samples, it was noted that the as received sample consists a mixture of α and β Ti with the β -Ti

relatively lower in volume fraction than the α -Ti. However, the laser nitrided sample showed mainly a formation of TiN and few α -Ti through the XRD analysis. The microhardness results showed that the nitrided sample has a relatively higher hardness value at the surface layer than the as-received sample and decreases gradually as the depth increases to the substrate layer. By measuring the cell proliferation using the methylthiazol tetrazolium (MTT) assay test of the as received sample and the laser nitrided sample, it was observed that the cell proliferation/viability significantly improved by laser nitriding, which in hand, improved the biocompatibility. In conclusion, it was noted that laser nitriding caused formation of TiN dendrites in the α -Ti matrix. Moreover, the microhardness and the cell proliferation were improved in the nitrided layer.

2.4 Corrosion Resistance Improvement

The microstructure characterization of Ti-6Al-4V nitride by Nd:YAG pulsed laser and the study of its corrosion resistance in an oxidizing acid environment consisting nitric acid was carried out by Razavi et al [17]. The Ti-6Al-4V samples were nitride using Nd:YAG pulsed laser in a pure nitrogen environment. The surface phase before and after the immersion tests were identified using XRD analysis. A 4M

HNO₃ solution was used for the potentiodynamic and cyclic polarization tests. Microstructure micrographs showed that the dendritic structures produced by the laser nitriding could be divided into three main regions, laser-melted region, heat affected region, and the base metal. XRD results before the immersion tests showed that the thin top layer consists mainly of TiN and small amount of TiN₀₃. The untreated and treated Ti-6Al-4V samples were immersed in a HNO₃ solution. Under the same immersion duration, the tests results showed that the weight loss of the untreated sample was less than the treated sample; this is because of the removal of the TiN layer and exposing the dendritic layer beneath it to the nitric acid solution. Polarization tests concluded that the TiN outer layer is the deciding factor in the protection of the laser nitride samples. Thus, the removal of this layer reduces the corrosion resistance. The cyclic polarization tests showed that the treated and untreated samples had high pitting corrosion resistance. However, the removal of the TiN layer in the treated samples lowered the pitting corrosion resistance. In conclusion, it was shown that the laser gas nitriding of Ti-6Al-4V was an effective surface modification method to improve the tribological properties. However, the thickness and continuity of the TiN outer layer is an important factor for the corrosion resistance of the nitride samples.

2.5 Titanium Nitriding in the Atmosphere

The oxidation prevention during laser processing of titanium and the hydrodynamic phenomena in laser nitriding were presented by Xuekang et al. [18]. The key component for nitriding in the atmosphere is to use a nozzle through which nitrogen jet was discharged onto the irradiated surface. A pulsed Nd:YAG laser as a laser source was introduced through the nozzle. The titanium alloy surface was nitrided without any noticeable oxidation under optimized nitriding conditions. TiN formation and dendrite structure were confirmed using XRD and SEM. Experiments were extended to include different flow rates of nitrogen and it was found that low flow rates results in improved nitriding quality. The proper design of the nozzle creates a high-pressure zone above the irradiated area and laminar flow which is important to protect the surface from the surrounding air and thus avoiding oxidation. It is important to note that maintaining a stable flow for laser nitriding through controlling the processing parameters is necessary to obtain reproducible results.

The study of surface morphology and coating components of titanium surface nitriding using laser and nitrogen plasma in the atmosphere was carried out by Yu et al [19]. Industrial pure titanium samples were used in the laser and plasma nitriding process, in which the

CW-CO₂ laser and the plasma gun were fixed coaxially to nitride the samples in the atmosphere with varying the process parameters. Morphology details and nitrogen content of the nitrided layer were obtained by SEM and XRD examinations. From the XRD analysis, it was found that relatively high power density, slow scanning speed and high plasma flow rate lead to better performance nitrided layer containing TiN, Ti₂N and Ti₄N_{2.33}. SEM micrographs showed dendrites in the nitrided area, below which, was the heat affected zone (HAZ). It was found that the larger size of HAZ lead to easier formation of cracks. EDS results showed that maximum nitrogen concentration was achieved at shallow depth and dropped sharply until the depth of the transition layer, in which, a gradual decrease in the nitrogen concentration was observed. In conclusion, surface nitriding obtained by laser and nitrogen plasma in the atmosphere was successful. As nitrogen plasma provided the nitrogen ions, surface nitriding can be achieved in the atmosphere at a relatively low laser power density when compared to laser nitriding. Consequently, laser and plasma nitriding was found to be an efficient method to incorporate nitrogen in the irradiated substrate when compared to laser nitriding.

2.6 Literature Survey Summary

Nitrided layer quality, microhardness, wears resistance, and corrosion resistances are considered the critical properties, which are affected by the nitriding process parameters. The development in the laser nitriding process in order to achieve optimum quality and properties is greatly influenced by the literature studies in the past. Most of the studies revealed that the nitrided layer mainly contains high concentration of TiN and few α -Ti at the surface. However, this concentration decreases with increasing depth in the layer. Moreover, several studies concluded that the presence of TiN in the nitrided layer improved the hardness and the wear resistance of the layer. Furthermore, the laser nitriding process parameters, i.e. laser power rate, scanning speed, nitrogen flow rate, and type of laser used, had a great effect on the characteristics of the resultant layer, in addition to forming a crack-free layer. Few studies showed that laser nitriding could be successfully achieved in an atmospheric environment. Additionally, studies show that the thickness and uniformity of the TiN outer layer plays an important role in the corrosion resistance of the nitride layer in a nitric solution.

The surface roughness of the laser nitrided Ti-6Al-4V alloy is, in general, high, which limits the potential application of the process.

However, PVD TiN coating on the laser treated surface may reduce the surface roughness and forms a hard surface on the treated layer. In the open literature, this issue was not addressed in details. Consequently, the objective of this thesis is to investigate the laser gas assisted nitriding and the TiN coating of the laser nitrided surfaces. The metallurgical changes in the TiN coated and nitrided layer are examined in details.

CHAPTER – 3

Equipment and Procedure

3.1 Introduction

In this chapter, the equipment used in this research are explained together with the experimental procedure. The equipment used include TiN coating apparatus, laser source, material characterization equipment, three-point bending and the hardness tests facilities. The topics are represented under the relevant sub-headings.

3.2 PVD TiN Coating

Chemical Vapor Deposition (CVD) and Physical Vapor Deposition (PVD) are considered to be the two major coating processes. These techniques provide effective control of thickness, coating composition and porosity. Vacuum or arc evaporation, sputtering, and ion plating are the three basic types of PVD processes. In general, these processes are carried out in high vacuum at temperatures in the range of 200-500 °C.

To produce thin layers of TiN on Ti-6Al-4V substrate surfaces, the following steps were incorporated: the ground, polished, and ultrasonically cleaned samples of Ti-6Al-4V were put into a PVD unit. By using a d.c magnetron source in an argon gas atmosphere, the

titanium film was sputter deposited onto the substrate at 260°C. Then it was implanted with N⁺ ions at 50 keV acceleration potential. After the implantation process, vacuum annealing was carried out at 540°C for one hour. A series of normal constant thickness single layer of 400 nm film was formed. The total thickness of the multi-layer film in the range 2-4 μm was obtained after a series of trials. The coat interface lattice parameters varied between 4.22Å and 4.275Å. Aluminum atoms have substituted some titanium in the lattice, which decreases the lattice parameter. The coverage area of defect is less than 1% of the surface after examining the SEM results.

3.3 Workpiece Material (Ti-6Al-4V alloy)

The material used for the workpieces is the Ti-6Al-4V alloy. This alloy contains aluminum αstabilizing element by 6% wt. and vanadium βstabilizing element by 4% wt. Table-3.1 presents the elemental weight percentages of the Ti-6Al-4V alloy

Element	Ti	Al	V	Cu	Cr	Fe	O
Amount (wt.%)	Bal.	6	4	0.03	0.01	0.32	0.20

Table-3.1 Chemical composition of Ti-6Al-4V Alloy (wt. %)

The mill annealing process resulted in a microstructure of α and intergranular β . The workpieces were cut into a rectangular shape, with dimensions of 30 mm x 150 mm x 5 mm. Later, they were ground and polished with 0.25 μ m alumina suspension, then degreased in acetone and dried in air before being treated. The peak-to-valley surface roughness was measured as 0.5 μ m workpieces.

3.4 Material Characterization

Appropriate sectioning, mounting and mechanical polishing was performed on the specimens in order to prepare them for the scanning electron microstructural investigation. The following etchants were used to reveal the features of the treated regions: -

[3 ml HF + 6 ml HNO₃ + water] or

[20 ml HF + 20 ml HNO₃ + 40 ml Glycerol]

The resulted microstructures were studied and recorded using optical microscopy and SEM. In order to prevent charging of the sample surface during the SEM photography, and to increase the contrast for higher resolutions, a sputtered layer of gold film was sputtered on the workpiece surfaces.

3.4.1 SEM and EDS

The purpose of SEM and microphotography are to provide high resolution and high magnification images of solid samples to show surface structure in order to investigate the metallographic changes in the nitride and nitride/melted regions, while the purpose of energy dispersive spectrometer (EDS), is to give quantitative and qualitative elemental analysis of the microscopic regions imaged to obtain the elemental distribution in respective regions.

JEOL JSM-6460LV scanning electron microscope with an X-ray detector was used for the SEM and EDS analyses in this thesis, as shown in Figure-3.1. It has a resolution of 0.3 nm, magnification range from 5x to 300,000x, and an accelerating voltage in the range of 0.3 – 30 kV.



Figure- 3.1 JEOL JSM-6460LV scanning electron microscope

3.4.2 X-ray Diffraction Analysis

The layers were analyzed by XRD using MoK α radiations after the nitriding process. XRD profiling of the treated cases were performed by periodic removal of the surface by SiC abrasive papers grinding. The analysis of the nitride species in the melted and untreated regions was carried out by Bruker XRD D8 Advanced (Figure- 3.2), with a typical setting of 40 kV and 30 mA.

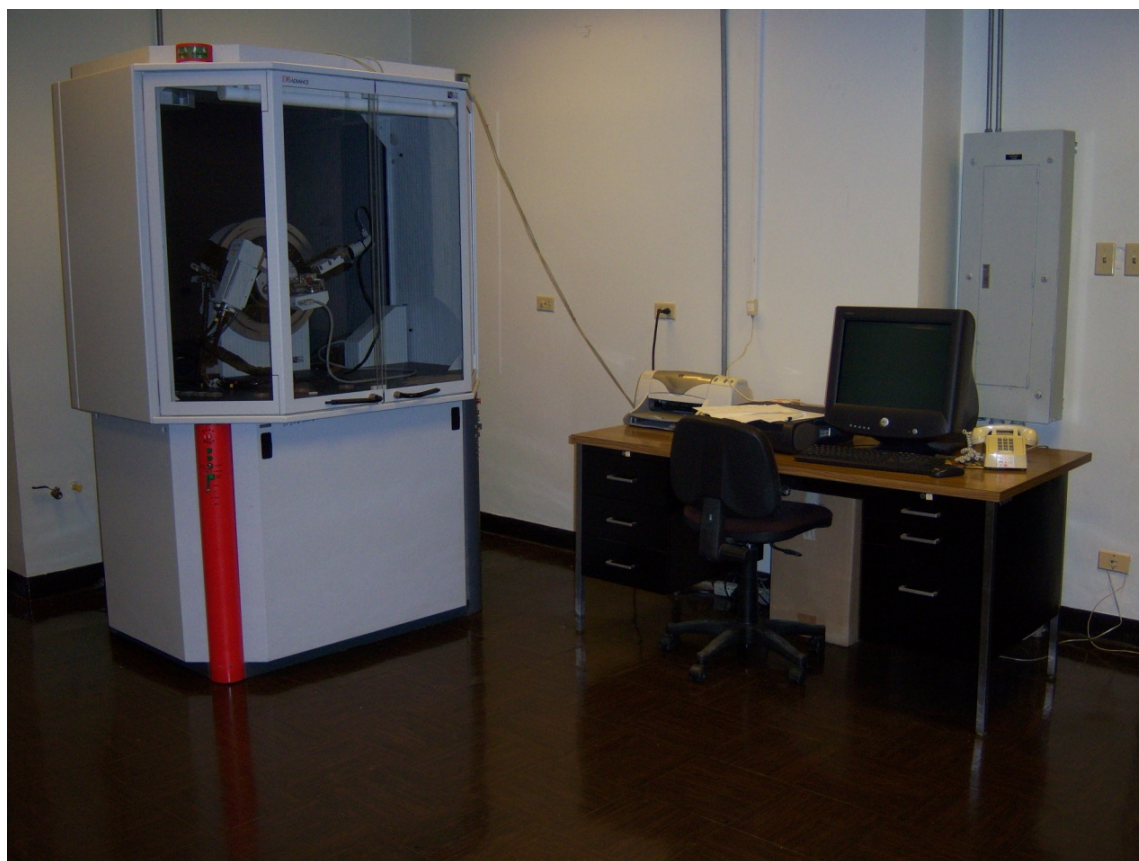


Figure- 3.2 Bruker XRD D8 Advanced.

3.5 CO₂ Laser Melting

Laser machining is considered to be part of the family of material removing or machining processes. Besides it involves special applications such as micromachining, it also provides a practical production method for hard-to-machine materials. However, when it comes to material removal rate and surface quality, laser machining has some limitations when compared to traditional machining methods. Even so, the interest of using lasers in welding, soldering, surface modification, marking, cutting, hole drilling and scribing is growing.

In surface melting process, the laser is used to successively melt a controlled area of the surface. During the cooling cycle of the process, solidification occurs which results in metallurgical properties different to conventionally cooled surfaces. This may provide high ductility and high strength together with good wear and corrosion properties of the substance [20,21]. Although grain refinement is always possible, some of the alloys cannot result in the optimum effect by surface melting. The particle injection, laser surface nitriding, cladding and surface alloying have been also introduced to improve the tribological properties of the surface [22, 23,24].

The Amada CO₂ laser (LC-ALPHAIII) delivering nominal output power of 2 kW at pulse mode with different frequencies was used to

irradiate the workpiece surface. The nominal focal length of the focusing lens was 127 mm. Nitrogen assisting gas emerging from a specially designed conical nozzle and co-axially with the laser beam was used. The experimental set up of the laser process is shown in Figure- 3.3, while the nitriding conditions are given in Table- 3.2.

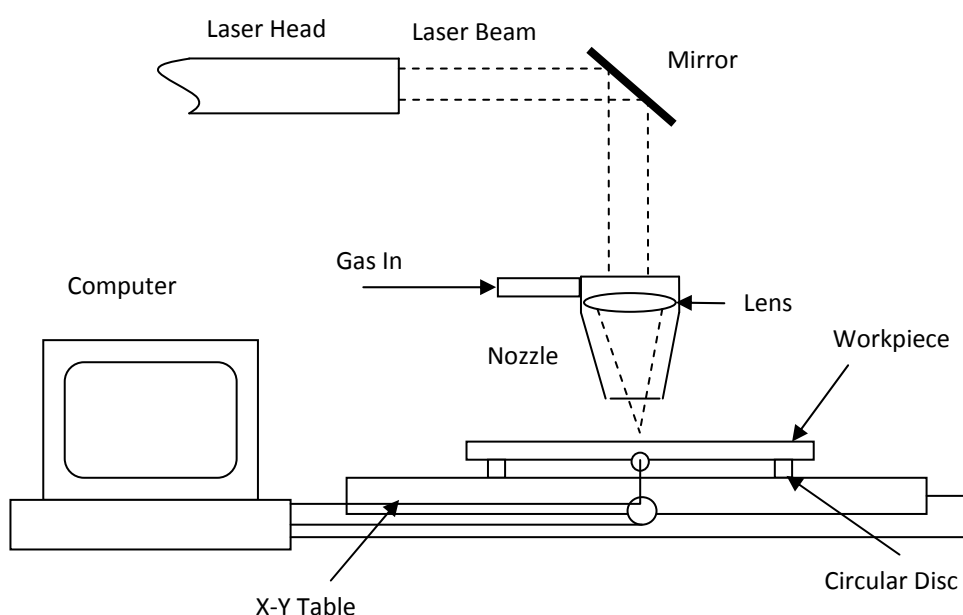


Figure- 3.3 Experimental Set-up

Feed Rate (mm/min)	Power (W)	Frequency (Hz)	Nozzle Gap (mm)	Nozzle Diameter	Focus Setting	N ₂ Pressure (kPa)
1000	70 and 110	1500	1.55	1.5	127	600

Table- 3.2 Laser assisted nitriding conditions

3.6 Hardness Tests

The hardness test is considered one of the most common tests for assessing the mechanical properties of material. The resistance to permanent indentation generally defines the hardness of a material. Also, the size or depth of the resulting indentation is measured, which in turn related to a hardness number.

The micro-hardness of the workpiece cross-section was measured using the Vickers tester, which uses a pyramid-shaped diamond indenter with the load kept at 300gm. The micro-hardness measurements were carried out across the workpiece cross-section before and after the nitriding process. The standard test method for Vickers indentation hardness of advanced ceramics (ASTM C1327-99) was used.

3.7 Three Point Bending Tests

The three point bending test is a mechanical test in which the specimen rests on two supports and a loading nose applies the load at a midway point between the supports. As per the three point bending test standard [ASTM D-790], the specimen is deflected until a maximum strain reaches 5% or until rupture occurs in the outer surface of the specimen [25].

Rectangular laser nitrided and laser nitrided and TiN coated specimens on the three point support fixture. The load and displacement characteristics were recorded during the tests. The tests were terminated when the treated layer reaches 5% of its flexural strain or when the layer failed. The bending strength (σ_b) of the laser nitrided and laser nitride and TiN coated samples was calculated by the below equation:

$$\sigma_b = \frac{3PL}{2bd^2} \quad (1)$$

where L is the span, P is the break load, b is the sample width, and d is the sample thickness.

The INSTRON 8801 dynamic loading machine manufactured by Instron Ltd. Co. was used. It has 100 kN load cell, hydraulic grips and a standard 50mm extensometer.

3.7.1 Determining Young's Modulus by Three Point Bending

The detailed formulation of Young's modulus was presented in the previous study [25], therefore only the governing equations are presented. After assuming the symmetry during the bending tests in relation to Figure-3.4, Young's modulus can be written as:

$$E_c I_c + E_s I_s = \frac{Pl^3}{48d} \quad (2)$$

Or

$$E_c = \frac{Pl^3}{(48d)I_c} - E_s \frac{I_s}{I_c} \quad (3)$$

Where I_c and I_s are the moment of inertia of the coating and the substrate material, l is the distance between the supports, P is the applied load, and d is the displacement of the substrate material and the coating during the bending tests. The moment of inertia of the substrate material and the coating are:

$$I_s = \int_{-h_s/2}^{h_s/2} y^2 b dy \text{ and } I_c = \int_{-h_s/2}^{(h_s/2)+h_c} y^2 b dy \quad (4)$$

where b is the width of the coating and the substrate material. Table- 3.4 and equation 3 are used to determine the Young's modulus of the coating. Due to the fact that the coating is applied on one side of the specimen, a non-symmetric situation along the central plane of the specimen resulted. Therefore, a shift of $\frac{h_c}{2}$ occurred in the axis of symmetry. This small shift was omitted in the calculations, which results into a small error in the calculations.

The related error to the load displacement characteristics obtained from the three point test measurements is in the order of 3%. The measurement errors are based on the data obtained from five experimental repetitions.

Figure-3.4 shows a schematic view of the three point bending test and the relevant dimensions.

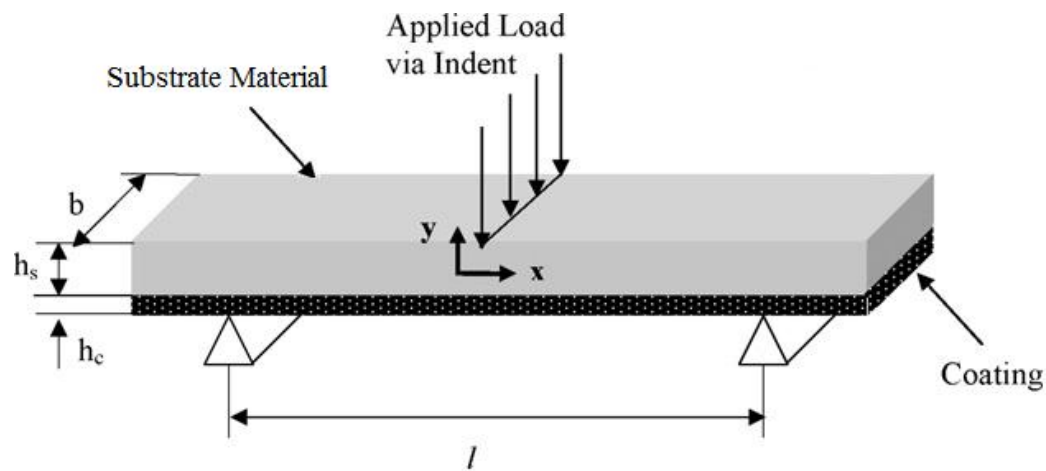


Figure- 3.4 A schematic view of the three point bending test

	Laser Nitrided and Coated Section	Laser Nitrided Section
h_s (m)	0.003	0.003
h_c (m)	0.000074	0.00076
P (N)	8100	8140
l (m)	0.0265	0.0265
d (m)	0.00064	0.00065
b (m)	0.01875	0.01875
I_s (m ⁴)	4.2 E-11	4.2 E-11
I_c (m ⁴)	4.6 E-13	4.5 E-13

Table- 3.3 Data used in the calculations of Young's modulus from three-point bending tests.

CHAPTER-4

Mathematical Analysis for Laser Melting

4.1 Introduction

The lump parameter technique can be used to model the laser heating and re-melting of coating, while solving the heat transfer equation yields the temperature distribution caused by the laser heating process. By using the momentum equations in the lump parameter technique, the molten front velocity is derived when the energy balance in the coating during the heating process is being considered. When using the Laplace transformation technique, the solution of the heat conduction equation for temperature distribution is achieved. Because the laser absorption depth and the focused spot diameter of the laser beam at the coating surface are significantly small, one dimensional heating situation is considered during the heating analysis for temperature formulation, i.e. temperature gradient along the radial direction is much lower than the temperature gradient along the beam axis in the substrate material.

4.2 Melt Depth Formulation

The influence of assisting gas, including cooling and exothermic reaction contribution on the melting process, has to be included in the model study. It is essential to note that the liquid layer film and the liquid film velocity at liquid film-assisting gas interface, including the assisting gas jet affect, should be determined in line with the laser surface treatment process. The exothermic reaction contributes to the energy transport process at the interface even with small amount of oxygen in the heating environment. Also, during the melting process, the assisting gas forms a boundary layer flow over the liquid film surface (molten metal surface) and heat transfer from liquid surface to boundary layer flow occurs, at assisting gas-liquid interface, because the assisting gas (nitrogen) is at room temperature, heat transfer from liquid surface to solid substrate occurs at liquid-solid interface. High temperature oxidation reaction at the melt surface provides excess energy to the laser irradiated region during the heating process. The liquid layer thickness is formulated in the appendix in line with the previous study [26]. Therefore, the equation for liquid layer thickness is presented below[26]:

$$\delta_L = \mu_L \frac{\sqrt{\frac{C_1}{C_5} s - \frac{5(C_4 + 2U_e^2)}{4 C_5}}}{\frac{1}{2} C_f \rho_g U_e^2} \quad (5)$$

Where

$$C_1 = \frac{1}{\rho_L} \frac{\frac{P_o}{A} - h(T_m - T_{oi})}{[Cp_s(T_m - T_i) + L_m + \beta L_{ev} + 1.65 Cp_m(T_{ev} - T_m)]}$$

And

$$C_2 = \rho_L [Cp_s(T_m - T_i) + L_m + \beta L_{ev} + 1.65 Cp_m(T_{ev} - T_m)]$$

And

$$C_4 = \rho_g U_e C_H [Cp_g(T_{ev} - T_{oe})]$$

And

$$C_5 = \frac{s}{2C_2} - \frac{1}{2} \mu_L \frac{1}{C_f \rho_g} \frac{2}{U_e^2}$$

A computer program in Mathematica software is developed to compute the liquid layer thickness (δ_L) from equation (5) for various power settings within the range 200 – 500 W. Table 4.1 gives the simulation conditions

Property	Value	Units
Boiling temperature	3030	K
Assisting gas velocity	130	m s ⁻¹
S	10 ⁻³	m
Melting temperature	1900	K
Density of assisting gas	1.19 at 150 kPa	kg m ⁻³
Density of workpiece	4570	kg m ⁻³
Fraction of evaporation contribution (β)	0.01	-----
Specific heat capacity of solid	523	J kg ⁻¹ K ⁻¹
Specific heat capacity of melt	560	J kg ⁻¹ K ⁻¹
Specific heat capacity of gas	918	J kg ⁻¹ K ⁻¹
Surface tension	1.5	N m ⁻¹
Thermal conductivity of molten metal	21.3	W mK ⁻¹
Thermal conductivity of solid	20.4	W mK ⁻¹
Latent heat of melting	418680	J kg ⁻¹
Latent heat of boiling	6.10 x 10 ⁶	J kg ⁻¹
Viscosity	0.35 x 10 ⁻²	N s m ⁻¹

Table- 4.1 Workpiece and assisting gas properties used in the simulations

CHAPTER – 5

Results and Discussion

Laser gas assisted nitriding of Ti-6Al-4V alloy is considered and microstructural changes in the irradiated region are examined using SEM, EDS, and XRD. The melt layer thickness developed during the process is formulated using the lump parameter analysis. The laser gas nitrided surfaces are, then, TiN coated using the PVD coating facility. The mechanical properties of the laser nitrided and laser nitrided and TiN coated workpieces are examined through three-point bending tests

Figure-5.1 shows melt depth predicted with laser output power. It can be seen that melt depth varies almost linearly with increasing laser output power. This is true for both assisting gas jet velocities. It should be noted that the nozzle exit velocity is studied in the simulations, i.e. pressurized nitrogen emerges from the conical nozzle and discharges into the environment before reaching the workpiece. This, in turn, results in attainment of high jet velocities at the nozzle exit. Moreover, increasing jet velocity lowers the melt layer thickness. This is associated with the convection losses from the free surface of the irradiated workpiece. Therefore, enhancement of heat transfer coefficient at the surface enhances the heat loss from the irradiated region while lowering the melt

layer thickness. The experimental data is in agreement with the predictions; however, some discrepancies are observed between the experimental data and the predictions. This can be attributed to the lump parameter analysis, which is adopted in formulating the liquid layer thickness. In this case, the analysis does not accommodate details of heat loss and gain, which may be obtained through the solution of the Fourier heat transfer equation. In addition, all the properties are assumed to be uniform and independent of the temperatures in the analysis. The maximum error estimated in the experimental results is in the order of 3%, since SEM micrographs are used for the depth layer measurements, i.e. main source of the error is based on the non-uniformities in the melt depth. Nevertheless, the predictions are in good agreement with the experimental results.

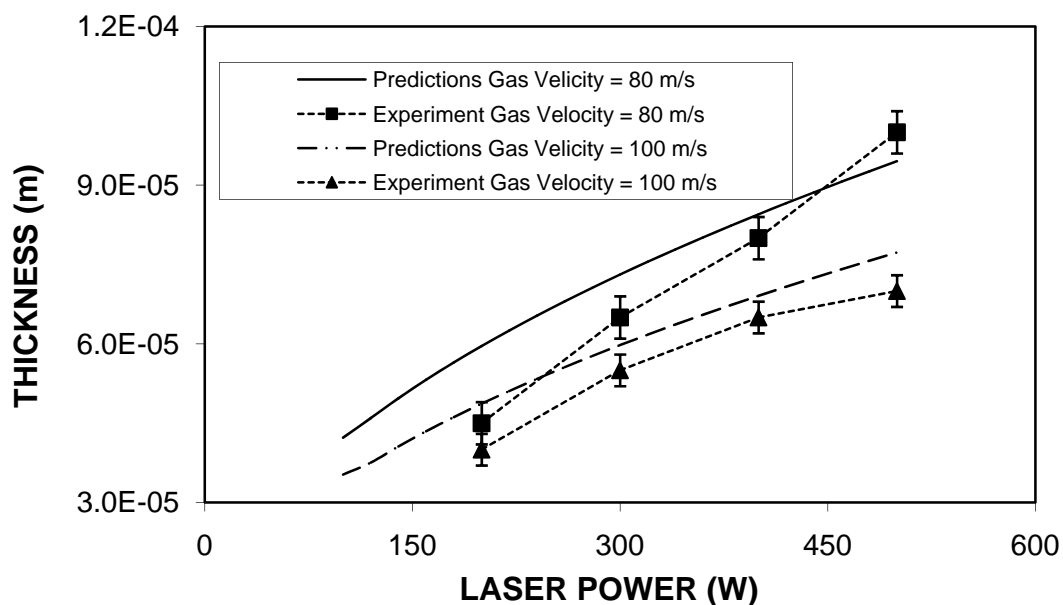
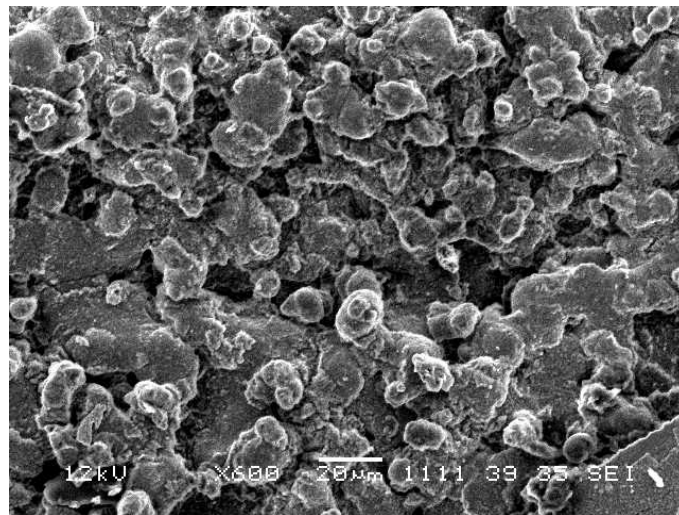
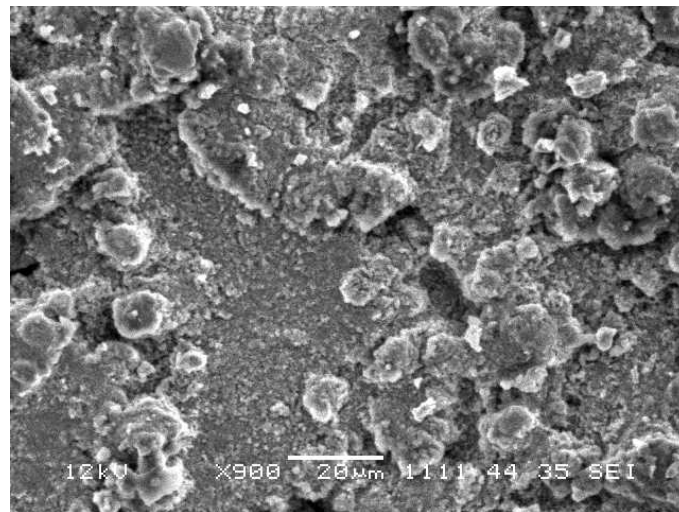


Figure- 5.1 Melt depth thickness with laser power intensity

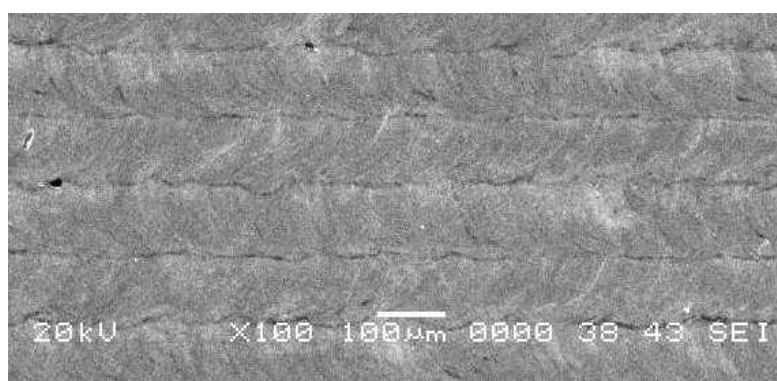
Figure-5.2 shows SEM micrographs for the top surfaces at laser nitrided and nitrided- TiN coated surfaces. It can be seen that laser nitriding results in rough surfaces. The melted and partially evaporated surface appeared as protruding columns. This structure is rich in nitride compounds; therefore, it is hard to remove. Moreover, it is also observed that the surface is free from cracks and cavities (due to evaporation). Consequently, micro-stress levels generated due to nitride compounds formation and thermal loading are not beyond the critical stress limits to form the cracks. However, it is evident from the visual inspection that the coloration at the surface after TiN coating; in which case, coated surface becomes more gold color as compared to laser nitrided surface. The laser melting tracks are evident and the overlapping ratio of the laser spots is over 80%. This provided almost smooth and continuous melting tracks at the surface. However, the spacing between tracks is 90% of the laser spot radius. This results in the melt front forming curvatures in the transverse direction, which is normal to the laser scanning direction. Since nitrogen gas pressure is high, oxidation at the surface due to high temperatures is not possible during the melting process.



Laser nitrided



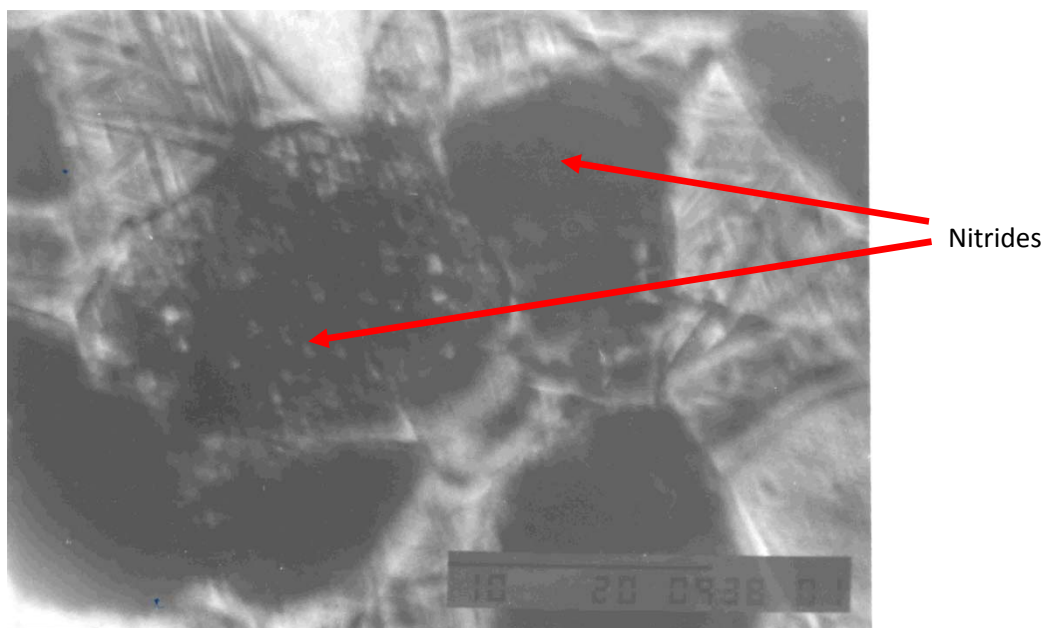
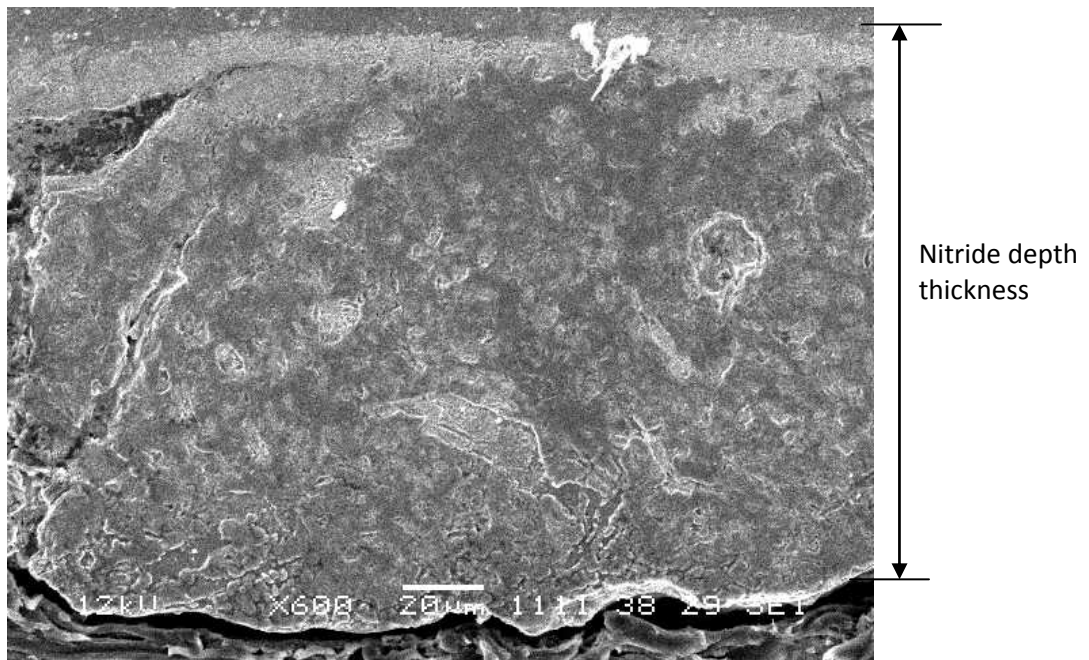
Laser nitrided and TiN coated



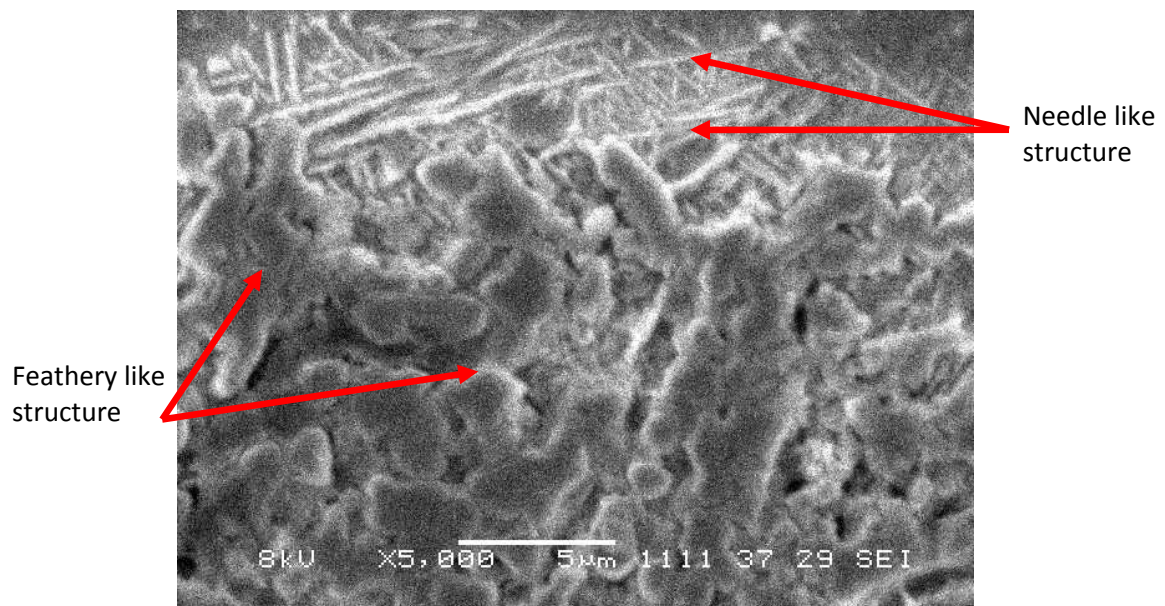
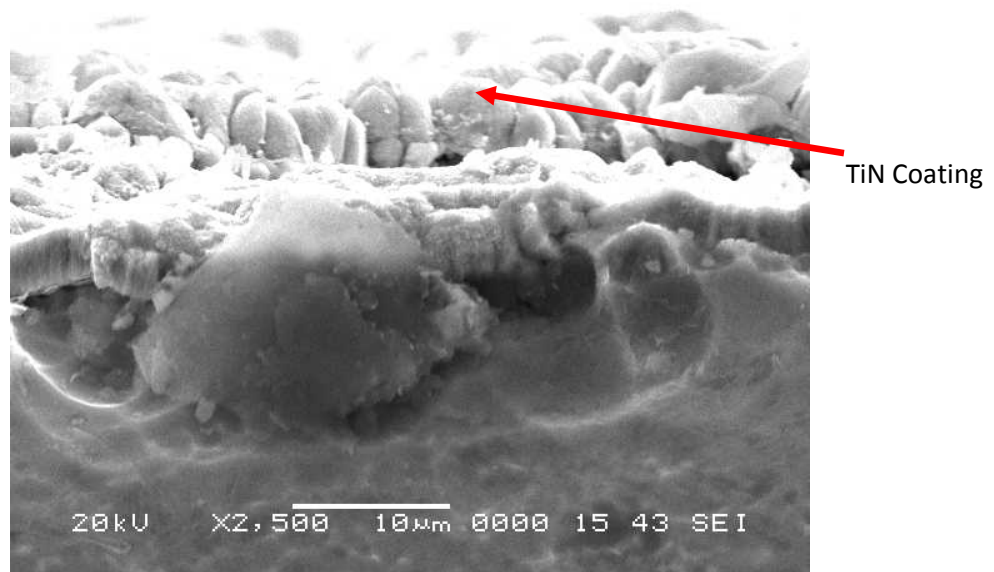
Patterns of laser scanning at the surface

Figure- 5.2 SEM and optical micrographs of top surface of laser nitrided and laser nitrided and TiN coated workpieces

Figure-5.3 shows SEM micrographs for the cross-sections of the laser nitrided and laser nitrided as well as TiN coated surface. It can be seen that the laser nitrided region extends almost 80 μm below the surface, which is in agreement with the model predictions (equation 5). The nitrided layer cross-section is free from defects including porosity, microcracks, voids, and large cavities. The nitride compounds formed in the surface region appears as feathery-like small structures. As the depth below the surface increases, the transition region is formed; in which, the size of the feathery-like structure increases. However, as the depth below the surface increases further, needle-like structure is formed. This region represents the end of the nitride layer and beginning of the heat affected zone. Since the region with the needle-like structure is small, the heat affected zone is also small. This is associated with the processing speed, which is significantly higher than that corresponding to the plasma nitriding process, e.g. laser gas assisted nitriding ends within seconds while plasma nitriding ends in the order of tens of hours. The orientation of needle-like structures is non-uniform, which can be caused by non-uniform cooling rates during the nitriding process.



(a)



(b)

Figure- 5.3 SEM micrographs of cross-section of (a) laser nitrided and (b) laser nitrided and TiN coated workpieces

Figure- 5.4 shows XRD diffractograms as-received and laser nitrided surfaces. As- received Ti-6Al-4V alloy composes of α -Ti and β -Ti; however, the majority phase is α -Ti. The presence of δ -TiN and ε -TiN peaks indicates that nitride-rich compounds are formed in the surface region. The presence of TiN (200) δ is due to the PVD coating, which is applied after laser nitriding process. However, Ti₂N peaks indicate the existence of transition zone between the nitride-rich surface and the base material. In this case, nitrogen concentration reduces significantly in this region. Increasing laser power results in shift in TiN (200) δ peak. This indicates that the probed inter-planar spacing is longer for the high laser power intensity than that corresponding to the low laser power intensity. The difference in 2θ represents the presence of compressive stress.

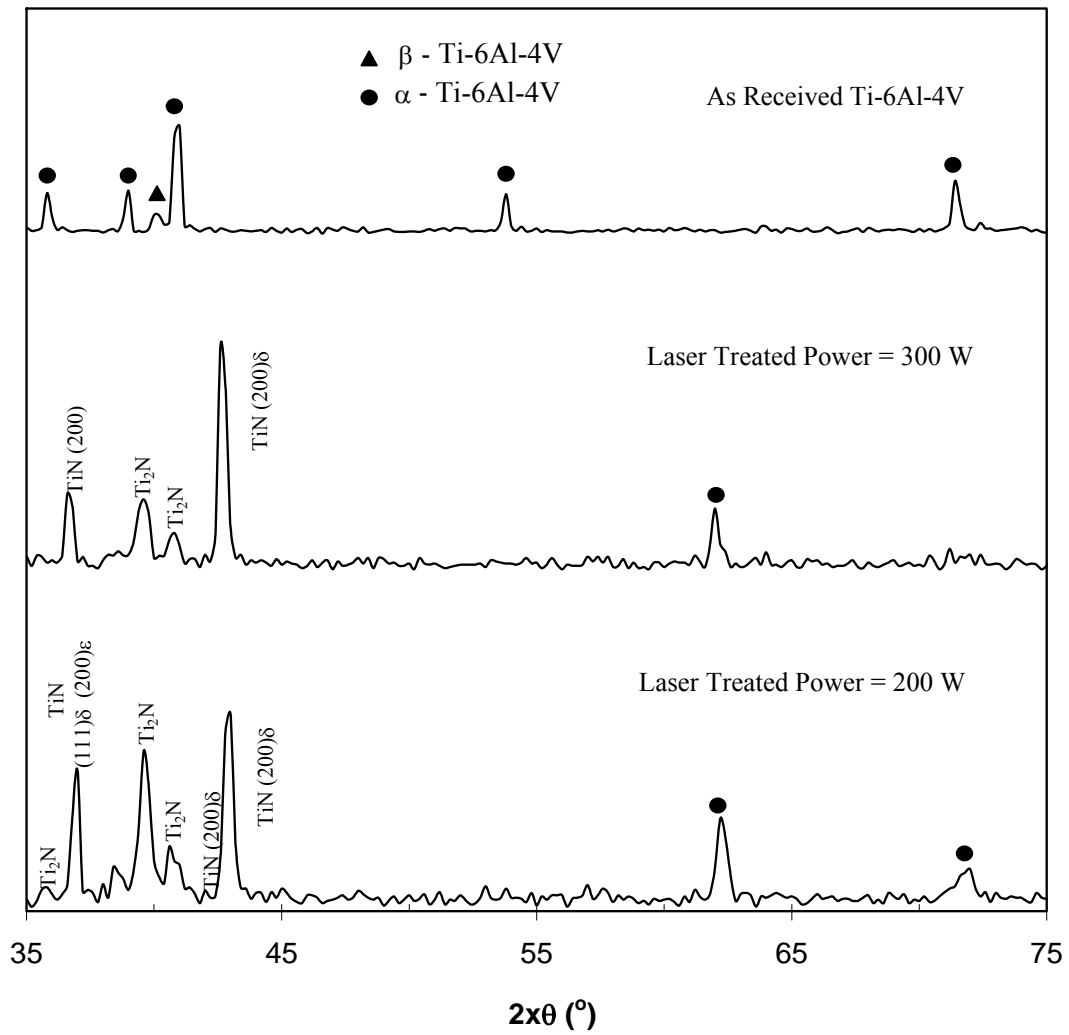


Figure- 5.4 XRD diffractogram for laser nitrided workpiece

Figure-5.5 shows microhardness variation inside the substrate material with TiN coated and uncoated laser nitrided surfaces. It is evident that microhardness attains higher values at the surface for TiN coated and laser nitrided surface than that corresponding to laser nitriding only. This is because of the presence of δ -TiN phase for the coated surfaces. However, δ -TiN and ϵ -TiN compounds are formed in the surface region of the laser nitrided workpiece. This is because of the

residual compressive stress developed in δ -TiN, which enhances the surface hardness [29]. As the depth below the surface increases, hardness reduces first gradually to about 25 μm below the surface. As the depth below the surface increases further, hardness reduces sharply to reach the base material hardness. The sharp decay in hardness is because of the decay of nitrogen concentration with increasing depth. Moreover, the transition region starts at about 25 μm below the surface.

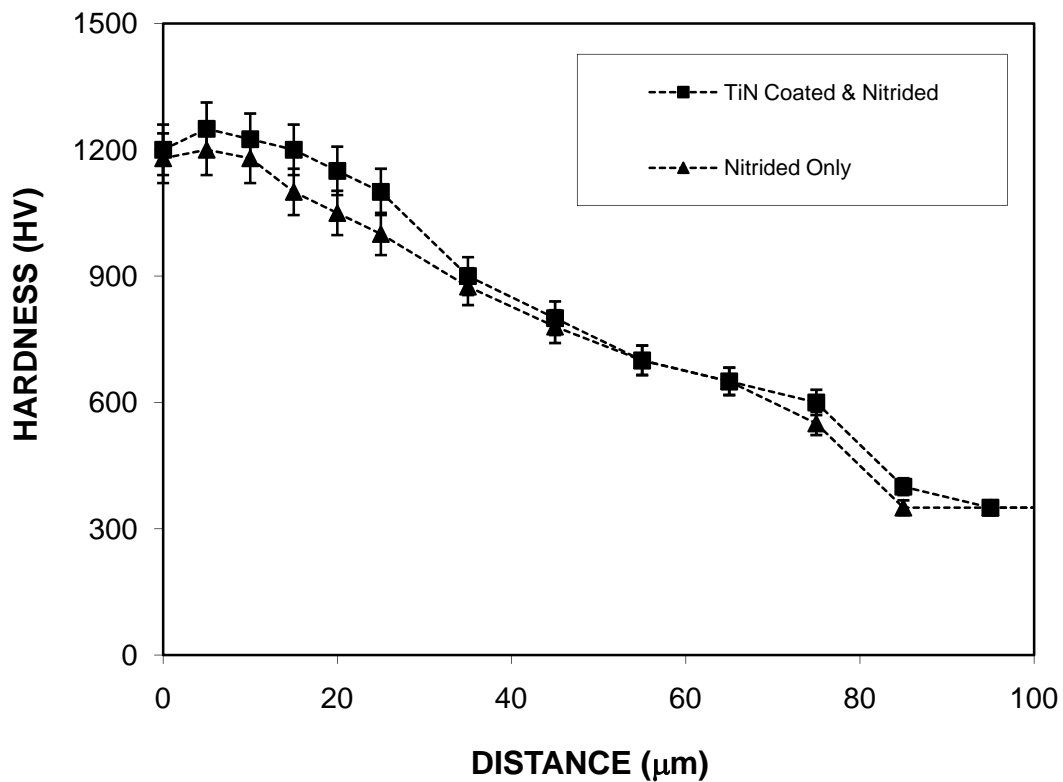


Figure- 5.5 Microhardness distribution inside laser nitrided workpiece

Figure- 5.6 shows SEM micrographs of laser nitrided and laser nitrided and TiN coated surface. It is evident that nitride formation in the surface region modified the surface texture and fine nitride structures are formed at the surface. This results in the surface roughness (R_a) in the order of $2.6\text{ }\mu\text{m}$. The surface roughness of the laser treated and laser treated and TiN coated workpieces are shown in Figure-5.7. Consequently, the cavity formation during the laser nitriding process did not take place. When comparing the surface roughness due to laser nitriding and laser nitriding and TiN coating, it appears that both surface roughnesses are in the same order. The difference is relatively small ($0.2\text{ }\mu\text{m}$). Therefore, TiN coating of the nitrided surface does not alter the resulting surface texture of the workpiece. This may be because of the TiN coating thickness, which is in the order of $2\text{ }\mu\text{m}$. As shown previously in Figure- 5.3, it should be noted that the nitrogen diffusion is limited with the surface region, since the diffusion coefficient is considerably small [31]. Therefore, nitrogen diffusion ceases at some depth below the surface. However, due to the high cooling rates, heat affected zone below the laser treated region is very narrow and no demarcation line is visible within boundary of the heat affected zone.

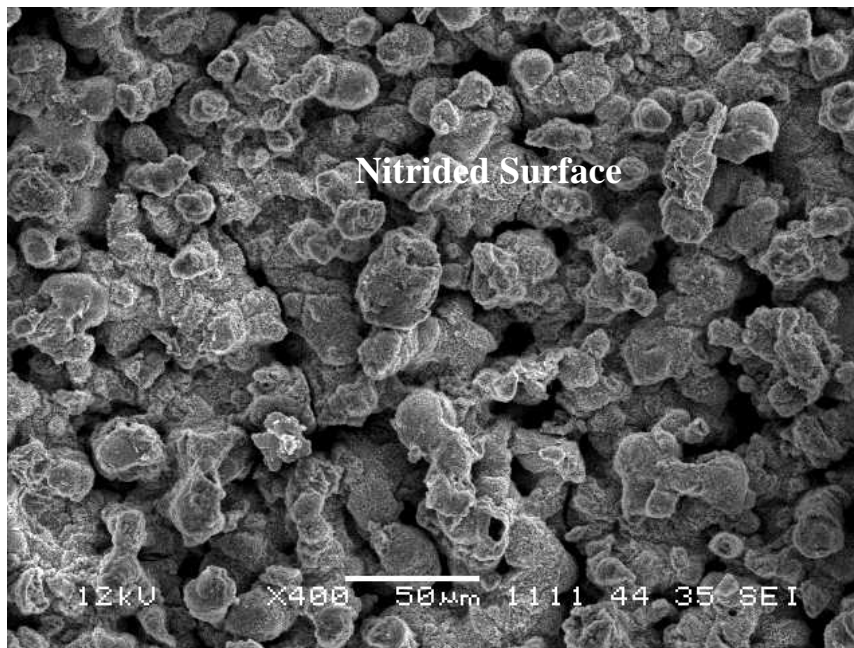
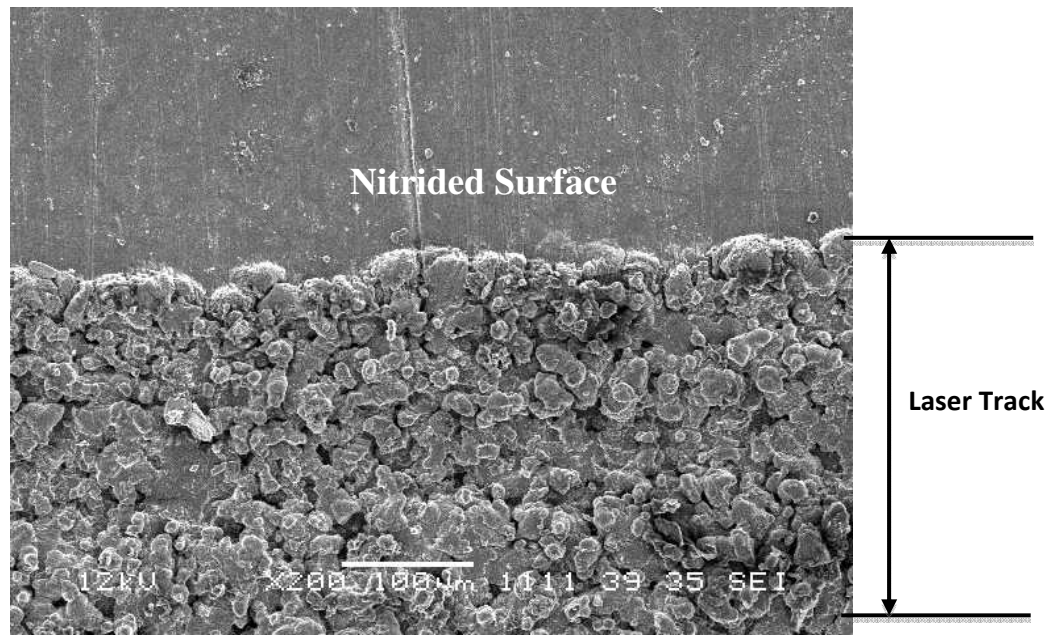


Figure- 5.6. Top view of laser nitrided surface.

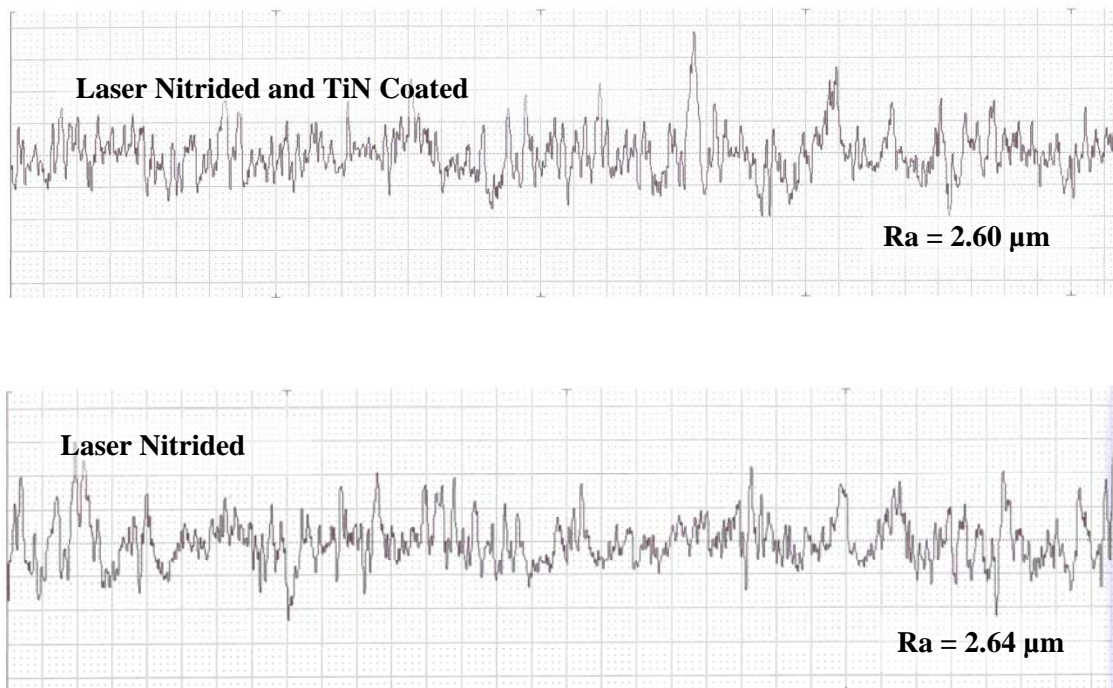


Figure- 5.7 Surface roughness of laser nitrided and TiN coated, and laser nitrided workpiece surfaces.

Figure-5.8 shows the bending load with the flexural displacement for the laser treated and laser treated and TiN coated workpieces. It should be noted that the bending data is obtained from the tests conducted at constant strain rate. Table- 5.1 gives the elastic modulus determined from the three bending tests. The laser nitrided and TiN coated surfaces resulted in slightly higher elastic modulus than that corresponding to the laser nitrided surfaces. This is attributed to the nitrided rich layer developed at the interface of the TiN coating and laser nitrided surface. It should be noted that to achieve 2 μm TiN thick coating on the laser nitrided surface, the laser nitrided workpiece is kept at 260°C

for almost four hours in the coating unit. This gives rise to excessive nitrogen diffusion in the surface vicinity of the laser nitrided workpiece. Consequently, bending load and flexural displacement characteristics changes for TiN coated and laser nitrided workpiece. This, in turn, results in some small differences in the Young's modulus between laser nitrided and laser nitrided and TiN coated workpieces as observed from Table-5.1. Moreover, the abnormal behavior in the bending curves is not observed, which suggests that the gradual deterioration of the laser treated and coated regions. In this case, the gradual deterioration of the interface of the workpiece would relieve the stress levels of the interface; consequently, the compressive stress generated at the top surface and tensile-shear stress developed at the bottom surface does not result in the total failure of coating and laser treated surfaces, i.e peeling due to the elastic strain energy stored in the treated region and TiN coating is not observed.

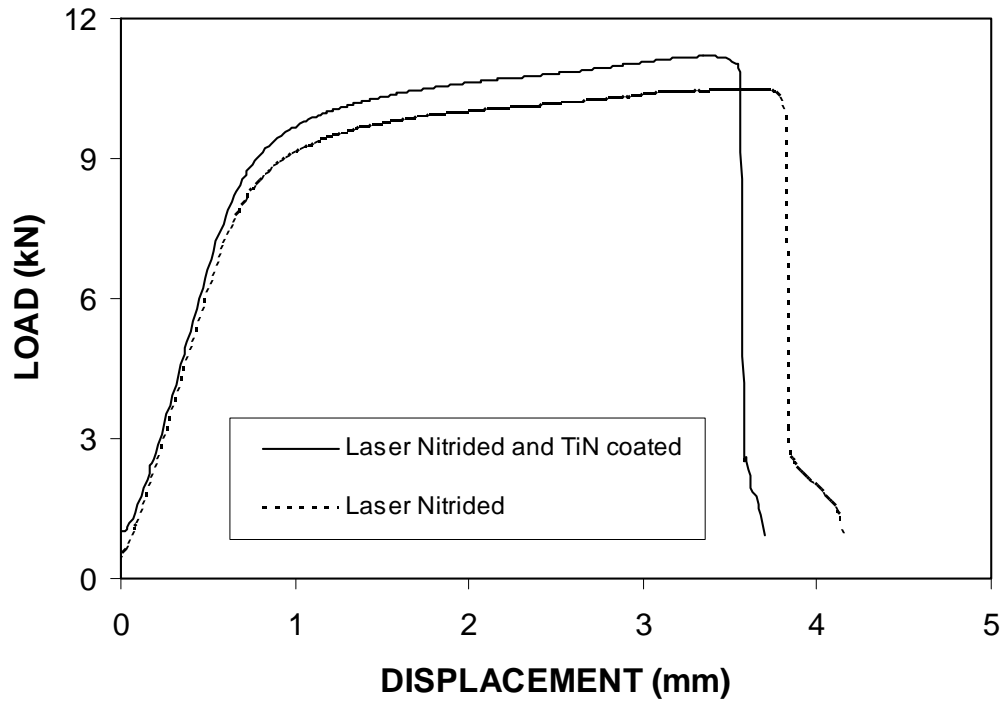


Figure- 5.8. Load displacement characteristics of three-point bending tests

	Laser Nitrided	Laser Nitrided and TiN Coated
Elastic Modulus (GPa)	453	555

Table- 5.1. Elastic modulus determined from three-point bending tests.

Figure- 5.9 shows optical and SEM micrographs of fractured surfaces after the three-point bending tests. Since the micrographs are taken from the bottom surface (opposite to the load applied surface), the laser nitrided and laser nitrided and TiN coated surfaces are subjected to tensile-shear force. The failure of the laser treated surfaces is due to the tensile-shear deformation; in which case, cracks are formed in the

surface region of the bended workpieces. The multi cracking including local separation of the surfaces are observed. The multi cracking for TiN coated and laser treated surface appears to be severe, which is due to the brittle structure of the TiN coating. Therefore, the shear stress developed at the interface of TiN coating and the laser nitrided surface is responsible for the multi-cracking in TiN coating. Moreover, the shear stress developed at the interface also initiates and contributes to the crack formation in the laser nitrided surface. In the case of laser nitrided surface, deep cracks are developed due to the tensile-shear loading in the surface region. However, the multi cracking is partially reduced with the deep and extended cracking in the surface region. This is attributed to the initial crack formation in the surface region which in turn results in stress relaxation in this region. As the bending progresses, the rate of shear strain increases while accelerating the crack propagation in the surface region. This causes deep penetration of cracks into the surface as well as the crack elongation in the surface region, i.e. the crack formed in the surface region minimizes the new crack formation in this region; therefore, multi-cracking replaces with the deep and elongated cracks in the surface region.

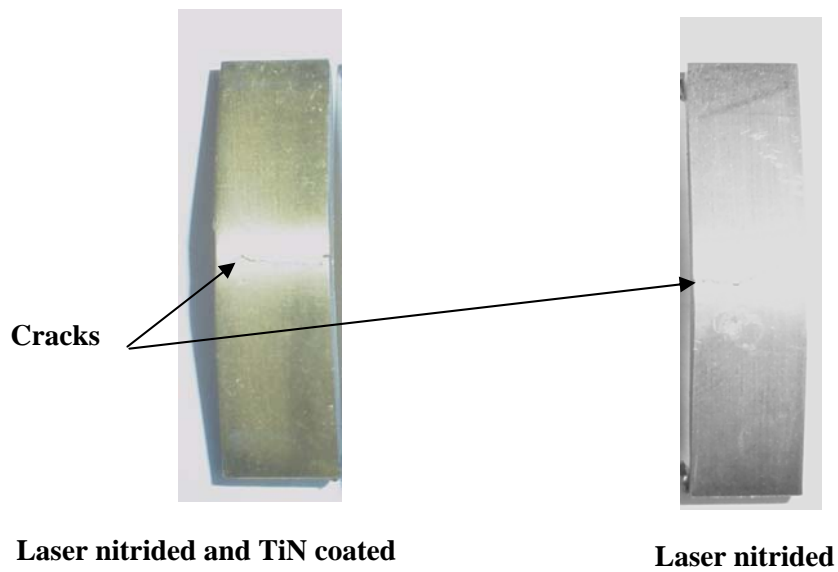
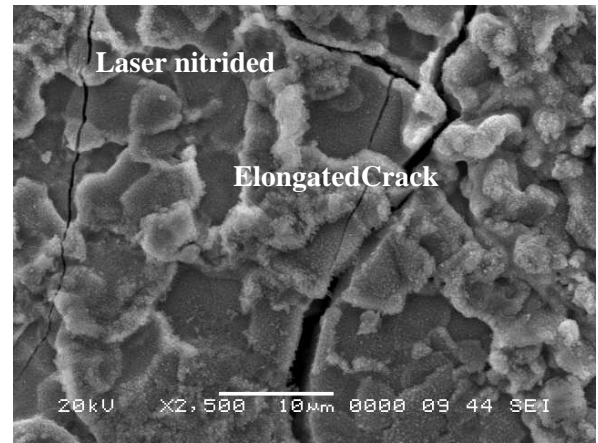
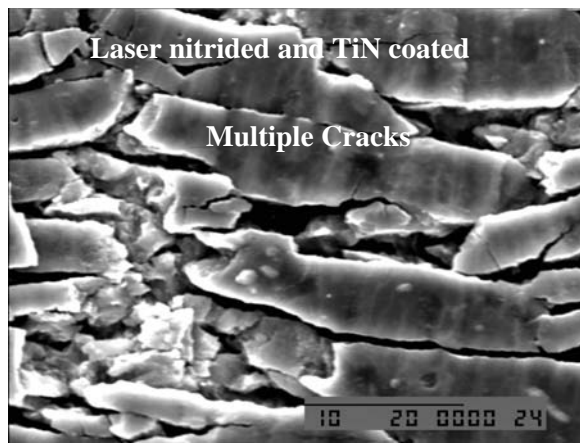


Figure- 5.9. SEM and optical micrographs of surfaces after three-point bending tests.

CHAPTER – 6

Conclusions and Future Work

Laser gas assisted nitriding of Ti-6Al-4V alloy is carried out and microstructural changes in the laser irradiated region are examined using SEM, EDS, and XRD. Laser nitrided surface is coated with TiN using the PVD facility. The TiN coating is carried out to develop a protective layer to corrosive environments. Moreover, the three-point bending tests are carried out and elastic modulus of the laser nitrided and TiN coated surfaces are determined

It is found that laser nitrided surface is free from cracks and other surface irregularities. The nitrided surface possesses partially protruding columns-like structures due to partial evaporation of the surface. These structures are rich in nitrogen due to nitride compounds formed in the surface region of the substrate material. TiN coating of the surface reduces the surface roughness of the resulting laser nitrided surfaces. The results of XRD diffractogram reveals that δ -TiN laser with mixture of ϵ -TiN phase is formed at the laser nitrided surface. The presence of TiN coating appears as δ -TiN peak in the diffractogram. The feathery-like structures are formed in the surface region of the workpiece showing the

nitride-rich structure. As the depth below the surface increases, this replaces with larger size feathery-like structure indicating the transition zone. As the depth below the surface increases further needle-like structure is formed, which is the indication of the heat affected zone. The depth of nitride layer extends almost 8 μm below the surface, which is in agreement with the model predictions. Increasing nitrogen gas pressure enhances the gas jet velocity at the exit. This increases the convective heat transfer from the surface while lowering the melt depth layer thickness. The microhardness of the TiN coated and laser nitrided surface is higher than that corresponding to laser nitrided surface. This is because of the compressive stresses developed in TiN coating. The depth of laser treated layer extends 80 μm below the surface. The elastic modulus determined from three-point bending tests reveal that the laser treated and TiN coated surfaces has higher elastic modulus than that corresponding to the laser nitrided surface. This is attributed to nitride enrichment of the surface during TiN coating process. The multi cracking is observed on the surface of the TiN coated and laser nitrided workpiece surface after the three-point bending tests. This is attributed to the tensile-shear stress developed at the interface of TiN coating and the laser nitrided surface. The brittle structure of TiN coating develops multi cracking in the coating and the shear stress developed at the interface

gives rise to the multi crack formation in the laser nitrided surface. In the case of the laser nitrided surface, deep and elongated cracks are observed after the bending tests. This is because of the initial crack formation and the compact structure formed in the laser nitrided surface. The initial crack formation results in the stress relaxation in the surface region; however, as the bending progresses, the rate of shear strain causes increased in concentration around the crack sites. This causes deep and elongated crack formation in the surface region. Consequently, the multi cracking replaces with the formation of the deep and elongated crack in the surface region.

Suggested Future Work

In the present work, laser gas assisted nitriding on Ti-6Al-4V was carried out, and the resulting surface was coated with TiN using PVD coating facility. The microstructural changes and morphology in the laser-irradiated area were examined using SEM, EDS and XRD. Also, the melt layer thickness in the surface region of the workpiece was formulated by introducing the mathematical modeling. Moreover, three-point bending tests were carried out in order to determine the elastic modulus of the laser nitrided and TiN coated regions at the workpiece surface. However, other material properties improvements when using laser nitriding and TiN PVD coatings are not investigated. Therefore, the following studies can be recommended for future work:

- Corrosion resistance of TiN coated and laser nitride surface.
- Wear and erosion resistance of case nitride surface.
- Three-dimensional modeling of heating, nitrogen diffusion and thermal stress developed when laser treated repair is carried out
- Influence of PVD TiN coating layer on the surface roughness of the laser nitrided region

Appendix

Mathematical Formulation of Laser Melting

The species formed after the chemical reactions (product of exothermic reactions) contribute to the heat transfer which takes place at gas-liquid interface. In this case, the ratio of dimensionless heat transfer coefficients due to diffusion (C_{H_d}) and chemical reaction (C_{H_c}) can be used to describe the heat transfer at the gas-liquid interface due to the high temperature oxidation reaction, which was presented as [27]

$$\frac{C_{H_d}}{C_{H_c}} = \frac{\left[1+B_1\left(\frac{U_L}{U_e}\right)\right]^{Pr-1}-1}{\left[1+B_1\left(\frac{U_L}{U_e}\right)\right]^{Sc-1}-1} \quad (A1)$$

Where

$$B_1 = \frac{2(\rho U)_g}{\rho_e U_e C_f}$$

and Pr is the turbulent Prandtl number and Sc ($Sc=\frac{\nu}{D}$) is the Schmidt number, where ν is the thermal diffusivity and D is the diffusion coefficient. U_e is the gas jet velocity at the outer edge of the assisting gas boundary layer (free stream velocity). U_L is the liquid velocity at interface, and C_f is the skin friction coefficient. When excluding the cooling effect and including the chemical reaction contribution of the

assisting gas, the rate of heat transfer per unit area of the molten metal (q_c), can be written as[27]:

$$q_c = \rho_e U_e C_{H_c} \left[\left(\frac{C_{H_d}}{C_{H_c}} - 1 \right) h_c \right] \quad (A2)$$

Where ρ_e is the gas density at the boundary layer edge, U_e is the gas velocity, and h_c is the chemical reaction enthalpy.

The ratio $\frac{C_{H_d}}{C_{H_c}}$ is dependent on Pr , Sc and B_1 where Pr and Sc are constants [27].

The energy balance related with the melting process can be simplified through investigating the melting process using lumped parameter technique. Thus, it is considered that the generated melt layer flows steadily in the direction of the assisting gas caused by the developed drag force at the assisting gas-liquid interface (figure A.1). Consider the generated melt layer at the solid surface during the steady laser heating process, and assume (β), a small fraction of molten metal evaporates from the surface at the assisting gas-melt interface during the laser heating process. Hence, the rate of energy required (\dot{E}_{req}) to generate a melt flow rate (\dot{m}_L) at the surface of the solid substrate can be written as:

$$\dot{E}_{req} = \dot{m}_L [Cp_s(T_m - T_i) + L_m + \beta L_{ev} + 1.65 Cp_m(T_{ev} - T_m)] \quad (A3)$$

Where T_m and T_i are the melting and initial temperatures of the solid substrate. L_{ev} and L_m are substrate material latent heating of evaporation

and. Cp_m and Cp_s are the specific heat capacity of the liquid and solid phases of the substrate. It should be noted that since the liquid layer flows along the surface due to a shear force across the gas-liquid interface, an extra rate of energy is stored. For that reason, $1.65Cp_m(T_{ev} - T_m)$ represents the extra rate of energy caused by the melt layer flow at the surface as approximated in the previous study [27]. Additionally, the rate of mass generated from solid into liquid at the solid surface in laser melting process can be written as:

$$\lim_{\Delta t \rightarrow 0} \frac{\Delta m}{\Delta t} = \frac{dm}{dt} = \dot{m}_L = \frac{d}{dt}(\rho \nabla) = \rho_L V_L A$$

where A is the cross section area, ρ_L is the density of melt, ∇ is the volume, and V_L is the liquid velocity along the y-axis (V_L is the velocity of melt generated from solid into liquid).

The rate of energy convective ($\dot{E}_{convection}$) from the surface caused by the assisting gas is :

$$\dot{E}_{convection} = \dot{m}_g C_H (h_o - h_g) \quad (A4)$$

where \dot{m}_g is the assisting gas mass flow rate, h_o is the total enthalpy ($h_o = \int_{T_{ref}}^{T_{ov}} Cp dT + \frac{1}{2} U_e^2$) at the boundary layer edge, and h_g is the total enthalpy ($h_g = \int_{T_{ref}}^{T_{ev}} Cp dT + \frac{1}{2} U_{LS}^2$) at assisting gas-liquid interface (where U_{LS} is the assisting gas-liquid interface velocity). As obtained from the Reynolds analogy, the heat transfer factor, C_H , is [28]:

$$C_H = \frac{1}{2} \frac{C_f}{Pr^{2/3}}$$

Where C_f is the skin friction coefficient and Pr is the Prandtl number ($Pr=0.7$). The evaluation of skin friction coefficient is based on the type of assisting gas flow. C_f can be evaluated as

$$C_f = 0.0576 Re^{-1/5}$$

in the case of turbulent boundary layer [28], where Re is the Reynolds number of the assisting gas flowing over the molten metal ($Re = 27000$).

As a result, the rate of energy input (\dot{E}_{in}) for melting at the assisting gas-liquid interface can be written as:

$$\dot{E}_{in} = P_o - \dot{E}_{convection} \quad (A5)$$

the laser power available at the assisting gas-liquid interface is represented by P_o . It should be noted that the reflectivity of the surface is included in the P_o , that is, P_o represents the laser power available after the reflection. As a result,

$$\dot{E}_{in} = P_o - \dot{m}_g C_H (\hbar_o - \hbar_g) \quad (A6)$$

On the other hand, the rate of heat transfer from liquid surface to assisting gas can be written as:

$$\dot{E}_{gas} = \dot{m}_g C_H (\hbar_o - \hbar_g) = \rho_g U_e A C_H \left[C p_g (T_{ev} - T_{oe}) + \frac{1}{2} (U_e^2 - U_{LS}^2) \right]$$

where A is the area, ρ_g is the assisting gas density, $C p_g$ is the specific heat capacity of the assisting gas at the edge of the boundary layer, C_H is

the heat transfer parameter, and T_{oe} is the gas temperature at the edge of the boundary layer.

Consider the rate of heat transfer from liquid to solid substrate across the liquid-solid interface; in this case, continuity of heat flux at the interface can be employed, i.e.:

$$\dot{E}_{conduction} = k_m \left[\frac{dT}{dx} \right]_m = A h (T_m - T_{oi}) \quad (A7)$$

Where k_m is the thermal conductivity of the melt layer, and $\frac{dT}{dx}$ is the temperature gradient at the melt-solid interface. Also, A is the area, h is the heat transfer coefficient at the interface, ($h = 3000 \frac{W}{m^2K}$) and T_{oi} is the solid temperature at infinitely large depth from the interface. It should be noted that across the liquid and gas interface, the conjugate heat transfer equation using Neumann boundary condition (continuity of heat flux and temperature) can be used. Since conjugate solution of the heating situation is simplified using a lump parameter analysis, the Neumann and radiation boundary conditions are omitted. As a result, a simplified approach is introduced employing a Dirichlet boundary at the interface (boundary condition of first kind).

(\dot{E}_{melt}) is the rate of energy required for melting:

$$\dot{E}_{melt} = P_o - \dot{m}_g C_H (h_o - h_g) - A h (T_m - T_{oi}) \quad (A8)$$

When setting the rate of energy balance across the melt per unit area, we get:

$$\frac{\dot{E}_{req}}{A} = \frac{\dot{E}_{melt}}{A} \quad (A9)$$

then:

$$V_L = \frac{1}{\rho_L} \frac{\frac{P_o}{A} - h(T_m - T_{oi}) - \rho_g U_e C_H [Cp_g(T_{ev} - T_{oe}) + \frac{1}{2}(U_e^2 - U_{LS}^2)]}{[Cp_s(T_m - T_i) + L_m + \beta L_{ev} + 1.65 Cp_m(T_{ev} - T_m)]} \quad (A10)$$

Consider the flow system as shown in Figure-A.1, the continuity equation for incompressible flow for the steady production of liquid substrate while neglecting the evaporation from the liquid surface during laser heating can be written as:

$$\frac{\partial U_L}{\partial s} + \frac{\partial V_L}{\partial y} = 0 \quad (A11)$$

where U_L represents the velocity of the liquid layer in the s direction. Only a small fraction (β) of melt evaporates.

Shear stresses should be the same at the assisting gas-liquid interface, In this case,

$$\tau_g = \tau_L$$

where τ_L is the shear stress exerted by the liquid layer on the gas layer, and τ_g is the shear stress exerted by an assisting gas on the liquid layer. If the liquid layer flow is assumed to be treated as due to extremely small liquid layer thickness, then the shear stress (τ_L) is:

$$\tau_L = \mu_L \frac{\Delta U_L}{\delta_L} \quad (\text{A12})$$

δ_L is the liquid layer thickness. $\Delta U_L = U_{LS}$ is the result for zero velocity at the solid surface, where U_{LS} is the liquid layer velocity at assisting gas-liquid interface. Hence, equation (A12) becomes:

$$\tau_L \approx \mu_L \frac{\Delta U_{LS}}{\delta_L} \quad (\text{A13})$$

The velocity distribution from in the liquid layer can be obtained from the momentum equations in the case of flow due to pressure variations with inclined surface. By assuming the liquid layer depth is considerably smaller than its width, the momentum equation for two dimensional flow is reduced to:

$$\frac{\partial^2 U_L}{\partial y^2} = \frac{1}{\mu} \frac{d}{ds} (P + \gamma z) \quad (\text{A14})$$

the angle inclination of surface is:

$$\sin \theta = -\frac{dz}{ds} \quad (\text{A15})$$

Due to considerably thin layer of liquid, assuming a linear variation of pressure in the liquid layer with constant slope along the s direction results in:

$$\frac{d}{ds} (P + \gamma z) = \text{Constant} \quad (\text{A16})$$

By solving equation (A14) with appropriate boundary conditions, the velocity distribution in the liquid layer becomes:

$$U_L = \frac{1}{2\mu} \frac{d}{ds} (P + \gamma z)(y^2 - y^5) + U_{LS} \left(1 - \frac{y}{\delta}\right) \quad (\text{A17})$$

Since $\frac{d}{ds} (P + \gamma z) = \text{constant}$ along the s direction, then:

$$\frac{\delta}{\delta s} \left(\frac{U_L}{U_{LS}} \right) = 1 - \frac{y}{\delta} \quad (\text{A18})$$

Also, the continuity of equation (A7) can be written as:

$$\int_0^y \frac{\delta V_L}{\delta y} dy = - \int_0^y \frac{\delta U_L}{\delta s} dy \quad (\text{A19})$$

or

$$\int_{V_0(0)}^{V_L(y)} dV_L = - \frac{d(\delta_L U_{LS})}{ds} \int_0^y \frac{U_L}{U_{LS}} \frac{dy}{\delta_L} \quad (\text{A20})$$

After inserting equation (A18) into equation (A20) and arranging it mathematically, equation (A20) becomes:

$$V_L(y) - V_L(0) = - \frac{d}{ds} \left\{ \delta_L U_{LS} \left[\frac{y}{\delta_L} - \frac{1}{2} \left(\frac{y}{\delta_L} \right)^2 \right] \right\} \quad (\text{A21})$$

given that $y = 0$ (at the assisting gas-liquid interface) $\Rightarrow V_L(0) = 0$ and $y = -\delta_L$ (at the liquid-solid interface) $\Rightarrow V_L(0) = V_L$. Then, reducing equation (A21) results in:

$$V_L = - \frac{d}{ds} \left(\frac{1}{2} \delta_L U_{LS} \right) \quad (\text{A22})$$

By substituting V_L from equation (A10), equation (A22) yields:

$$- \frac{d}{ds} \left(\frac{1}{2} \delta_L U_{LS} \right) = \frac{1}{\rho_L} \frac{\frac{P_o}{A} - h(T_m - T_{oi}) - \rho_g U_e C_H \left[C p_g (T_{ev} - T_{oe}) + \frac{1}{2} (U_e^2 - U_{LS}^2) \right]}{[C p_s (T_m - T_i) + L_m + \beta L_{ev} + 1.65 C p_m (T_{ev} - T_m)]} \quad (\text{A23})$$

Or:

$$-\frac{d}{ds}\left(\frac{1}{2}\delta_L U_{LS}\right) = C_1 - \frac{\rho_g U_e C_H \left[C p_g (T_{ev} - T_{oe}) + \frac{1}{2}(U_e^2 - U_{LS}^2) \right]}{C_2} \quad (A24)$$

Here, we have $C_1 = \frac{1}{\rho_L} \frac{\frac{P_o}{A} - h(T_m - T_{oi})}{[C p_s (T_m - T_i) + L_m + \beta L_{ev} + 1.65 C p_m (T_{ev} - T_m)]}$

and

$$C_2 = \rho_L [C p_s (T_m - T_i) + L_m + \beta L_{ev} + 1.65 C p_m (T_{ev} - T_m)]$$

The heat transfer characteristics accordingly due to the flow of the assisting gas over the melt surface. For this reason, the rate of heat transfer from the liquid surface to the assisting gas is modified as [28]:

$$\dot{E}_{gas} = N s^{-1/5} \quad (A25)$$

N is a function varying with \dot{E}_{gas} , it is considered to be constant along the s direction [28]. Therefore, equation (A24) becomes:

$$-\frac{d}{ds}\left(\frac{1}{2}\delta_L U_{LS}\right) = C_1 - \frac{N s^{1/5}}{C_2} \quad (A26)$$

By integrating equation (A26) we get:

$$-\frac{1}{2}\delta_L U_{LS} = \int \left[C_1 - \frac{N s^{1/5}}{C_2} \right] ds \quad (A27)$$

or:

$$-\frac{1}{2}\delta_L U_{LS} = C_1 s - \frac{5}{4} \frac{N}{C_2} s^{4/5} + C_3 \quad (A28)$$

The boundary conditions will determine the constant C_3 .

The velocity of the liquid surface is approximately zero at the tip of the cutting edge. Because the liquid layer thickness is negligibly small in this region. As a result, at $s = 0$: $U_{LS} = 0$; therefore, $C_3 = 0$.

By replacing $\dot{E}_{gas} = Ns^{-1/5}$ in equation (A28), we get:

$$-\frac{1}{2}\delta_L U_{LS} = C_1 s - \frac{5}{4} \frac{\rho_g U_e C_H [C p_g (T_{ev} - T_{oe}) + \frac{1}{2}(U_e^2 - U_{LS}^2)] s}{C_2} \quad (A29)$$

By defining the constant C_4 as:

$$C_4 = \rho_g U_e C_H [C p_g (T_{ev} - T_{oe})]$$

Equation (A29) becomes:

$$-\frac{1}{2}\delta_L U_{LS} = C_1 s - \frac{5}{4} \frac{C_4 s}{C_2} + \frac{1}{2} \frac{(U_e^2 - U_{LS}^2)s}{C_2} \quad (A30)$$

After re-arranging equation (A30), we get:

$$\frac{s}{2C_2} U_{LS}^2 - \frac{1}{2}\delta_L U_{LS} = C_1 s - \frac{(5C_4 + 2U_e^2)s}{4} \quad (A31)$$

Additionally, in order to obtain the liquid layer thickness, consider the shear stresses at the assisting gas-liquid interface, that is :

$$\tau_g = \tau_L \quad (A32)$$

$\tau_L = \mu_L \frac{U_{LS}}{\delta_L}$ from equation (A12), then τ_g can be written as:

$$\tau_g = \frac{C_f}{2} \rho_g U_e^2$$

After inserting the shear stresses in equation (A31), the liquid layer thickness becomes:

$$\delta_L = \mu_L \frac{U_{LS}}{U_e} \frac{2}{C_f \rho_g U_e^2} \quad (\text{A33})$$

The result of combining equations (A31) and (A33) is:

$$U_{LS} = \sqrt{\frac{C_1}{C_5} S - \frac{5}{4} \frac{(C_4 + 2U_e^2)}{C_5}} \quad (\text{A34})$$

where

$$C_5 = \frac{s}{2C_2} - \frac{1}{2} \mu_L \frac{1}{C_f \rho_g} \frac{2}{U_e^2}$$

The liquid film thickness in the melting section is obtained by substituting equation (A34) into equation (A33) [27].i.e.:

$$\delta_L = \mu_L \frac{\sqrt{\frac{C_1}{C_5} S - \frac{5}{4} \frac{(C_4 + 2U_e^2)}{C_5}}}{\frac{1}{2} C_f \rho_g U_e^2} \quad (\text{A35})$$

In order to compute the liquid layer velocity and liquid layer thickness in the cutting section, both equations (A34) and (A35) are used.

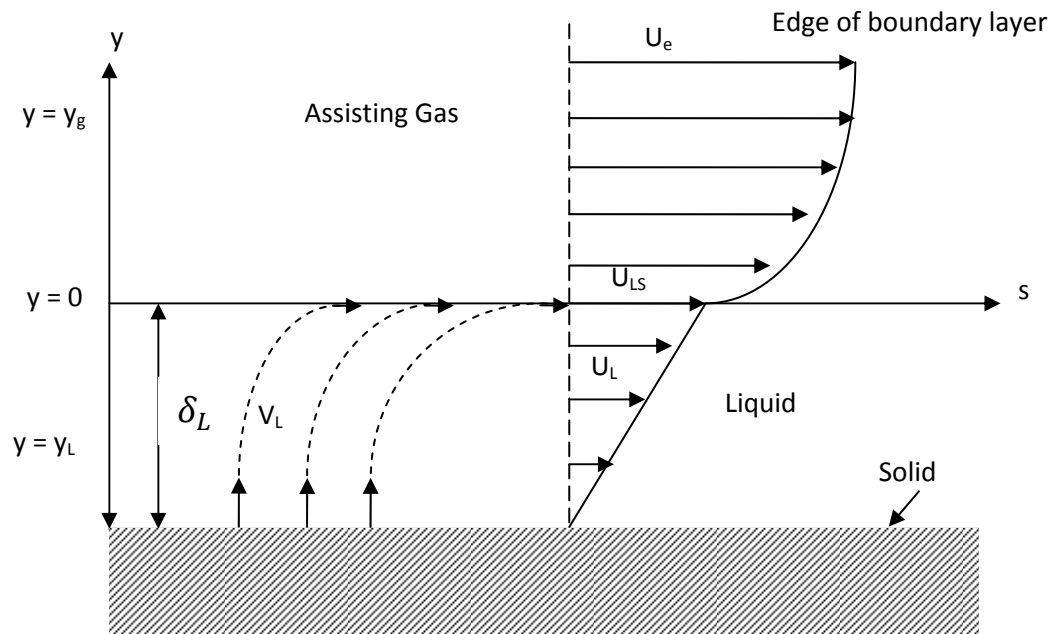


Figure- A.1 A schematic view of liquid and gas side velocities in the coordinate system

References

- [1] ASM Handbook: Properties and Selection : Nonferrous Alloys and Special-Purpose Materials (VOL. 2),Asm International,1990.
- [2] E.A. Avallone,T. Baumeister III, Marks' Standard Handbook for Mechanical Engineers,10th Edition, McGraw-Hill, 1996.
- [3] A. Zhecheva, W. Sha, S. Malinov, Adrian Long, Enhancing the microstructure and properties of titanium alloys through nitriding and other surface engineering methods, Surface & Coatings Technology 200 (2005) 2192–2207.
- [4] <http://steelguru.com/uploads/reports/sss3-29-08-2008.jpg>
- [5] J.H. Abboud, A.F. Fidel, K.Y. Benyounis, Surface nitriding of Ti–6Al–4V alloy with a high power CO₂ laser, Optics & Laser Technology 40 (2008) 405–414.
- [6] Y.L. Yang', G.J.Zhoand D.Zhang, Improving the surface property of TC4 alloy by laser nitriding and its mechanism ,Acta Metall. Sin. (Engl. Lett.) Vol. 19 No.2 pp 151-156 Apr. 2006.
- [7] A. Biswas, L. Li, U.K. Chatterjee, I. Manna, S.K. Pabi and J. Dutta Majumdar, Mechanical and electrochemical properties of laser surface nitrided Ti–6Al–4V,Scripta Materialia 59 (2008) 239–242.
- [8] H. Tahara, Y. Ando,Study of titanium nitride deposition by supersonic plasma spraying, Vacuum 83 (2009) 98–101.
- [9] E. Costa Santos, M. Morita, M. Shiomi, K. Osakada, M. Takahashi, Laser gas nitriding of pure titanium using CW and pulsed Nd:YAG lasers, Surface & Coatings Technology 201 (2006) 1635–1642.
- [10] B.S. Yilbas, M.S.J. Hashmi, S.Z. Shuja, Laser treatment and PVD TiN coating of Ti-6Al-4V alloy,Surface and Coatings Technology 140 Ž2001. 244–250.
- [11] Y. S. Tian, C. Z. Chen, L. X. Chen, and Q. H. Huo,Crack-free wear resistance coatings produced on pure titanium and ti-6Al-4V by laser, Surface Review and Letters, Vol. 12, Nos. 5 & 6 (2005) 741–744.

- [12] A.F. Yetim, A. Alsaran, I. Efeoglu, A. Çelik, A comparative study: The effect of surface treatments on the tribological properties of Ti-6Al-4V alloy, *Surface & Coatings Technology* 202 (2008) 2428–2432.
- [13] B.S. Yilbas, M. Sunar, Z. Gasem, B.J. Abdul Aleem, Laser gas assisted nitriding and tin coating of Ti-6Al-4V alloy: Experimental and numerical investigation of mechanical properties, *Journal Of Materials Processing Technology* 209 (2009) 1199–1208.
- [14] Yongqing Fu, Hejun Du, and Yanwei Gu, Improvement of Erosion Resistance of Titanium with Different Surface Treatments, *JMEPEG* (2000) 9:571-579.
- [15] S. Ettaqi, V. Hays, J.J. Hantzpergue, G. Saindrenan, J.C. Remy, Mechanical, structural and tribological properties of titanium nitrided by a pulsed laser, *Surface and Coatings Technology* 100~101 (1998) 428-432.
- [16] A. Biswas, U.K. Chatterjee, L. Li, I. Manna, and J. Dutta Majumdar, Laser assisted surface modification Ti-6Al-4V for bioimplant application, *Surface Review and Letters*, Vol. 14, No. 4 (2007) 531–534.
- [17] R.Sh. Razavi, M. Salehi, M. Monirvaghefi, G.R. Gordani, Corrosion behaviour of laser gas-nitrided Ti-6Al-4V alloy in nitric acid solution, *Journal of Materials Processing Technology* 203 (2008) 315–320.
- [18] X. Chen, G. Wu, R. Wang, W. Guo, J. Yang, S. Cao, Y. Wang, W. Han, Laser nitriding of titanium alloy in the atmosphere environment, *Surface & Coatings Technology* 201 (2007) 4843–4846.
- [19] H. Yu, F. Sun, J. Zhang, Laser and plasma nitriding of titanium using CW-CO₂ laser in the atmosphere, *Current Applied Physics* 9 (2009) 227–233.
- [20] W.M. Steen, Surface coating using as laser, *International conference of Advances in Surface Coating Technology*, London, Vol.1 (1978).
- [21] M.K. El-Adawi, M.A. Abdel-Naby and S.A. Shalaby, Laser heating of a two-layer system with constant surface absorption: An

- exact solution, *Int. J. Heat and Mass Trans.*, Vol. 38 (1995) 947-952.
- [22] B.L. Mordike, State of the art of surface engineering with high energy beams, *Key Engineering Materials*, 46-47 (1990) 13-26.
 - [23] K.G. Budinksi, Tribological properties of titanium alloys, *Wear*, 151 (1991) 203-217.
 - [24] D. Whitesed, R.E. Goffeith and M.N. Srinivdson, The effects of laser trimming on properties of Ti06Al-4V sheet, *Materials and Manufacturing process*, vol. 10 No. 6 (1995) 1201-1214.
 - [25] ASTM D 790, “Standard Test Methods for Flexural Properties of Unreinforced and Reinforced Plastics and Electrical Insulating Materials”, American Society for Testing and Material Standards, Philadelphia, (2003).
 - [26] B.S. Yilbas and B.J.A. Aleem, Dross formation during laser cutting process, *Journal of Applied Physics: Part D*, Vol. 39 (2006) 1451-1461.
 - [27] B.S. Yilbas and A. Z. Shahin, Turbulent boundary layer approach allowing chemical reactions for CO₂ laser oxygen assisted cutting process. *Proc. of Instn. Mech. Eng. C:J. Mech. Eng. Sci.* 208 (1994) 275-84.
 - [28] W.H. Dorrance, *Viscous Hypersonic Flow*, 1992, New York: McGraw-Hill.
 - [29] S.L.R. Silva, L.O. Kerber, L. Amaral and C.A. Santos, X-ray diffraction measurements of plasma-nitrided Ti-6Al-4V, *Surface and Coatings Technology*, Vol.116-119 (1999) 342- 346.
 - [30] B.S. Yilbas, M. Sunar, Z. Gasem, B.J. Abdul Aleem, S. Zainaulabdeen, Study into mechanical properties of TiN coating on Ti-6Al-4V alloy through three-point bending tests. *Industrial Lubrication and Tribology*, 58(2006) 68-71.

Publications by the Author

- O. Al-Mana, M.S.J. Hashmi, B.S. Yilbas, Laser gas assisted nitriding and TiN coating of Ti-6Al-4V alloy, conference on Advances in Materials and Processing Technologies, AMPT09, Kuala Lumpur, Malaysia, October 26-29, 2009.
- O. Al-Mana, M.S.J. Hashmi, B.S. Yilbas, Laser nitriding of Ti alloys and three point bending tests , conference on Advances in Materials Processing Technology, AMPT10, Paris, France October 24-27, 2010.